

國立臺灣大學工學院化學工程學系



碩士論文

Department of Chemical Engineering

College of Engineering

National Taiwan University

Master Thesis

功能性聚丙二醇－二腺嘌呤奈米顆粒性質研究

Functional nanoparticles of Poly(propylene glycol)-bis-Adenine

李舜傑

Shun-Chieh Lee

指導教授：李篤中 博士

Advisor: Duu-Jong Lee, Ph.D.

中華民國 104 年 7 月

July 2015

國立臺灣大學碩士學位論文
口試委員會審定書

功能性聚丙二醇-二腺嘌呤奈米顆粒性質研究
Functional nanoparticles of Poly(propylene glycol)-bis-Adenine

本論文係李舜傑君 (R00524061) 在國立臺灣大學化學工程學系
完成之碩士學位論文，於民國 104 年 7 月 23 日承下列考試委員審查
通過及口試及格，特此證明

口試委員：

李舜傑

(簽名)

(指導教授)

王大明

王大明

李舜傑

鄭智嘉

系主任、所長

王大明

(簽名)

(是否須簽章依各院系所規定)



誌謝

碩士研究過程中，我受到許多人的幫助；沒有他們，便沒有今日的成果。

研究方面，李老師每次在會議總能快速看出研究的問題點，靈活、跨領域的思考與洞察力總讓我佩服。也感謝老師提供許多機會讓我們練習說英文。鄭老師則提點合成、材料物性檢測的注意事項，給予研究方向及論文的建議。Chris 老師協助改進我的英文說寫，並從生物技術觀點提供建議。張國棟老師做學問的深度、廣度和態度是我看齊的目標。感謝黃志彬老師、朱曉萍老師提供論文修改建議。

技術方面，國領學長與子揚學長教我基本的實驗器具操作與安全注意事項。娛茹學姊教會我使用動態雷射光散射儀與螢光光譜儀。陳俊吉技術員指導動態雷射光散射儀與 zeta potential 之測量。政樺學姊分享高分子材料領域的研究經驗。吳夢婷技術員協助分析 MALDI-TOF 質譜。黃技術員協助 NMR 並提供樣品準備的建議。張美杏技術員協助 GPC 與離心機的操作。蔡逸峰技術員慷慨提供 TEM sample 用具及協助拍攝 TEM。王廷玉技術員以熟練的技術準備 Cryo-TEM 樣品及拍攝照片，並提供專業的解說與建議。泓錦學長提供 wafer 與指導使用 spin coater。許曉萍技術員協助拍攝 SEM 並提供諮詢。誌鍵學長指導使用 UV/Vis 分光光度計並提供測量建議。

生活方面，初入實驗室時，雅伶學姊的鞭策，讓我儘早接觸實驗的真實面貌。宓霓學姊與欣月學姊溫暖的鼓勵與接納，讓我漸漸不害怕進實驗室。特別感謝宓霓學姊在我尚未適應實驗室生活時主動關懷，消除了我的不安。翎翔、忠彥與冠儒在碩一上學期課業上與研究上的切磋，讓我不孤單。王蔚與麗霏不止是課業與生活上的好夥伴，一年半來更提供許多實驗上的點子與建議，找出我看問題的盲點，並在實驗不順時互相勉勵。建豪學長、雅鈞學姊、昱辰學長、佳貞學姊、Nikolai 學長協助我熟悉實驗室儀器與環境，也為我示範 meeting 與口試的報告方式。伯瑄、廷璋、威伶、拜石、軒宇各有所長，與他們聊天學習了不少技巧與知識，激發我的研究靈感。政樺、娛茹、宓霓三位學姊協助處理行政事務，讓我能專心於研究。實驗室的成員彼此閒聊、聚餐與出遊，都給我美好的回憶。

最感謝的是我的家人，全力支持我就讀碩士班。

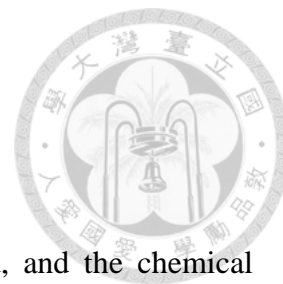


摘要



本研究合成並純化有機高分子材料「聚丙二醇－二腺嘌呤」，並以核磁共振、質譜儀與凝膠滲透層析法確立其結構。掃描式與穿透式電子顯微鏡，以及動態雷射光散射技術顯示聚丙二醇－二腺嘌呤溶於水中會形成奈米顆粒，其平均粒徑約為 100 奈米。聚丙二醇－二腺嘌呤的臨界微胞濃度(CMC)以芘(pyrene)的螢光光譜決定，其結果為 8×10^{-2} mg/mL。最低臨界溶解溫度(LCST)係以紫外光／可見光光譜儀測定，結果發現聚丙二醇－二腺嘌呤的最低臨界溶解溫度會隨其在水中濃度變化，且其在濃度越高時變化幅度越小。此材料最低臨界溶解溫度範圍涵蓋人體體溫。初步的藥物載入與釋放實驗顯示，此材料有很好的藥物包覆率與最低臨界溶解溫度附近快速的藥物釋放表現，有潛力作為標靶藥物傳輸之載體。

Abstract



The polymer PPG-bis-adenine was synthesized and purified, and the chemical structure was characterized by NMR, mass spectroscopy, and chromatography. Scanning electron microscopy, transmission electron microscopy and dynamic light scattering showed the existence of nanoparticles formed by PPG-bis-adenine, and the mean diameter of nanoparticles was determined to be about 100 nm in aqueous solution. The critical aggregation concentration was determined using pyrene fluorescent emission and was determined to be around 8×10^{-2} mg/mL. The LCST behavior is studied using UV/Visible spectrophotometer. It is found that the LCST is concentration-dependent, and the variation of LCST is less significant at higher concentrations. The LCST range covers human body temperature. Preliminary drug loading and release experiments revealed good entrapment efficiency and instant release of drug at LCST phase change, showing potential of PPG-bis-adenine as a targeted drug carrier.



Table of Contents

誌謝	i
摘要	ii
Abstract.....	iii
Table of Contents.....	iv
List of Figures.....	vi
List of Tables	viii
Abbreviations	ix
Chapter 1. Introduction	1
Chapter 2. Literature Review	2
2.1 Supramolecular Chemistry	2
2.2 Controlled Drug Release	4
2.2.1 The improvement of solubility for low-solubility drugs	4
2.2.2 Targeted delivery of drugs	5
2.3 Polymeric Nanoparticles.....	6
2.3.1 Hydrophobic Interaction.....	6
2.3.2 Shapes of aggregation of Amphiphilic Molecules.....	6
2.3.3 Amphiphilic Copolymers	8
2.3.4 Temperature-sensitive Copolymers as Carriers for Targeted Delivery	9
2.3.5 Drug loading and release	11
2.4 Poly(propylene glycol)	11
2.5 Nucleobases	12
Chapter 3. Materials and Methods	14
3.1 Synthesis of PPG-bis-adenine	14
3.1.1 The Addition Reaction.....	14
3.1.2 Purification by Column Chromatography	15
3.2 Nuclear Magnetic Resonance (NMR)	16
3.3 Gel Permeation Chromatography (GPC).....	16
3.4 Elemental Analysis	17
3.5 Mass Spectroscopy (MALDI-TOF-TOF).....	17
3.6 Critical Micelle Concentration (CMC) determination by pyrene fluorescence	18
3.7 Lower Critical Solution Temperature (LCST) determination by UV/Visible spectrophotometry	20

3.8	Mean diameter measurement by Dynamic Light Scattering (DLS)	22
3.9	Zeta potential measurement	23
3.10	Scanning Electron Microscopy (SEM)	23
3.11	Cryogenic Transmission Electron Microscopy (cryo-TEM)	24
3.12	Drug Loading and Release	25
Chapter 4.	Results and Discussion	27
4.1	Structure Characterization	27
4.1.1	NMR Spectroscopy	27
4.1.2	Mass spectroscopy & GPC	27
4.1.3	Elemental analysis	33
4.2	Evidence of Nanoparticles	36
4.2.1	Dynamic light scattering	36
4.2.2	Scanning Electron Microscopy	36
4.2.3	Cryo-TEM	41
4.2.4	Zeta potential	41
4.2.5	CMC determination	42
4.3	The LCST behavior	45
4.3.1	LCST determination by UV/Vis spectrophotometry	45
4.3.2	Mean diameter change around LCST	45
4.4	Drug loading and release	48
Chapter 5.	Conclusions and Future work	50
References	51



List of Figures

Figure 2-1	Relationship between critical packing parameter and shapes of aggregation of amphiphilic molecules.....	8
Figure 2-2	Phase diagram of a system exhibiting lower critical solution temperature .	9
Figure 2-3	Structure of Poly(propylene glycol)	12
Figure 2-4	Various modes of hydrogen bonding between nucleobases.....	13
Figure 2-5	Structures of nucleobases which occur in DNA	14
Figure 3-1	The reaction for the synthesis of PPG-bis-adenine.....	15
Figure 3-2	Color of solution below (left) and above (right) LCST	22
Figure 4-1	¹ H NMR spectroscopy of PPG-bis-adenine in CDCl ₃	29
Figure 4-2	Mass spectrum of (a) PPG 800 diacrylate (reactant) and (b) PPG-bis-adenine (product)	30
Figure 4-3	GPC chromatogram of PPG 800 diacrylate and PPG-bis-adenine	32
Figure 4-4	Theoretical carbon and hydrogen composition of PPG diacrylate as a function of degree of polymerization	34
Figure 4-5	Theoretical carbon and hydrogen composition of PPG diacrylate as a function of degree of polymerization	35
Figure 4-6	Variation of mean diameter of PPG-bis-adenine nanoparticles with temperature under 1 mg/mL	37
Figure 4-7	Variation of mean diameter of PPG-bis-adenine nanoparticles with temperature under 2 mg/mL	37
Figure 4-8	Variation of mean diameter of PPG-bis-adenine nanoparticles with temperature under 3 mg/mL	38
Figure 4-9	Variation of mean diameter of PPG-bis-adenine nanoparticles with temperature under 4 mg/mL	38
Figure 4-10	Variation of mean diameter of PPG-bis-adenine nanoparticles with temperature under 5 mg/mL	39
Figure 4-11	SEM image of nanoparticles of PPG-bis-adenine under 1 mg/mL.....	39
Figure 4-12	SEM image of nanoparticles of PPG-bis-adenine under 0.1 mg/mL	40
Figure 4-13	Cryo-TEM image of PPG-bis-adenine nanoparticles under 1 mg/mL	40
Figure 4-14	Zeta potential of nanoparticles of various concentrations of PPG-bis-adenine aqueous solution	42
Figure 4-15	Fluorescent emission of pyrene in different concentrations of PPG-bis-adenine solution. The intensity is normalized according to peak I.	43

Figure 4-16	CMC determination by the variation of “peak III to peak I” ratio	44
Figure 4-17	LCST determination by transmittance at 800 nm	46
Figure 4-18	Concentration dependence of LCST of PPG-bis-adenine	46
Figure 4-19	Mean diameter variation with temperature across LCST	47
Figure 4-20	Color change of PPG-bis-adenine solution across LCST	47
Figure 4-21	Calibration curve for pyrene concentration in drug loading experiment.	48
Figure 4-22	Pyrene fluorescent emission intensity change during the release-reload process	49



List of Tables

Table 3-1	Sample Concentrations for CMC determination	19
Table 4-1	Molecular weight of PPG 800 diacrylate and PPG-bis-adenine of various degrees of polymerization	31
Table 4-2	Theoretical atomic compositions of the reactant and the product.....	33
Table 4-3	Elemental analysis of the reactant and the product	33

Abbreviations

CMC	critical micelle concentration
Cryo-TEM	cryogenic transmission electron microscopy
DLS	dynamic light scattering
GPC	gel permeation chromatography
LCST	lower critical solution temperature
MALDI-TOF	matrix-assisted laser desorption ionization – time of flight
NMR	nuclear magnetic resonance
PPG	poly(propylene glycol)
PPG-bis-adenine	poly(propylene glycol)-bis-adenine
SEM	scanning electron microscopy
TEM	transmission electron microscopy





Chapter 1. Introduction

Targeted drug delivery has been an active research topic in the past decades. The advantage of targeted drug delivery includes less side effects and higher bioavailability, which are especially desirable in cancer treatment. There have been many methods dedicated to targeted delivery of cancer drugs, which exploit the unique microenvironment like higher temperature and lower pH of tumor cells. With “smart” materials which respond to temperature, pH, and other stimuli, cancer drugs can be protected and transported to target cells, then released by the microenvironmental stimulus of target cells. However, most of these stimuli-responsive copolymers have complex structures, have to be synthesized through many steps, and the precise degree of polymerization is hard to control. In this study, we utilized the flexibility of supramolecular chemistry to synthesize a temperature-responsive material, poly(propylene glycol)-bis-adenine (PPG-bis-adenine). PPG-bis-adenine has a simple structure and is easy to synthesize. It can self-assemble into nanoparticles above its lower critical solution temperature (LCST), and the nanoparticles disassemble above LCST. This makes PPG-bis-adenine a good candidate of drug carrier for controlled release. We studied its physical properties and explored its performance in drug loading and release.

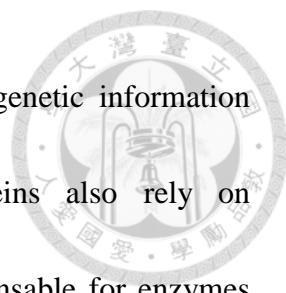


Chapter 2. Literature Review

2.1 Supramolecular Chemistry

Supramolecular chemistry is concerned with non-covalent interactions between molecules, such as hydrogen bonding, van der Waals force, metal-ligand coordination, π - π interaction, π -cation interaction and electrostatic force. Usually these interactions are not as strong as covalent bonds, so supramolecular structures are more flexible and constitutionally dynamic. When exposed to external stimuli like temperature or pressure change, these structures may change their shape and constitution accordingly, by destruction and reestablishment of non-covalent interactions, yet they are strong enough to form stable macrostructures [1]. The versatility of these non-covalent interactions offer many tools for chemical, biological, and engineering researches.


Supramolecular chemistry is closely related to self-organization, a process in which simple units form complex structures spontaneously. There are lots of examples of self-assembled macromolecules in biological systems. The basic structure of cell membranes is the lipid bilayer, amphiphilic lipids with hydrophobic tails enclosed between hydrophilic parts. These lipids are held together by van der Waals force and hydrogen bonding with each other and with proteins within the bilayer [2]. DNA double helices are stabilized by hydrogen bonding and π - π interaction between nucleobases,



and the precise base pairing between nucleobases is the key to genetic information storage [3]. Secondary and higher order structures of proteins also rely on intermolecular interactions, and these higher structures are indispensable for enzymes and structural proteins to function [4].

Biological supramolecular structures have inspired scientists to make synthetic macromolecules connected by non-covalent bonds. Traditionally, molecule synthesis involves stepwise linking and breaking of covalent bonds, but this approach becomes impractical for molecules of larger molecular weight; polymerization is the main strategy instead. For even complex molecules, non-covalent interactions have been incorporated in the synthesis processes [4], and the definition of “molecule” has been expanded to include non-covalent linkages. Some researchers demonstrated the synthesis of aggregate formed by hydrogen bonding between melamine and cyanuric acid [5], some used metal-ligand coordination to make geometrical macrocyclic structures [6, 7]. Hydrogen bonding and metal-ligand coordination have also been used in the bottom-up construction of nanostructures and devices [8-12]. Supramolecular chemistry has bridged the size gap between bottom-up processes like traditional organic synthesis, and top-down processes like photolithography [13].

Non-covalent interactions have also been exploited by scientists to mimic molecular recognition found in biological systems, as in the specific receptor-target and



enzyme-substrate relationship. Some metal-organic coordination frameworks possess porous structure and were utilized in specialized catalysis [14], such as chiral-specific catalysis [15], which can be used for chiral separation. Crown ethers and calixarenes were designed to selectively bind to specific ions using metal-ligand and π -cation interactions, particularly alkali-metal ions, heavy metals, and ammonium in amino acids [16-19]. Hydrogen bonding between melamine and cyanuric acid was used for the detection of melamine illegally added to milk [20].

2.2 Controlled Drug Release

2.2.1 The improvement of solubility for low-solubility drugs

Many drugs are insoluble in water. The insolubility reduces the bioavailability of drugs, and makes it hard to control the dosage [21]. One classification of drugs is according to the permeability and solubility. If the drug belongs to the class of high permeability and low solubility, the bioavailability can be improved by raising the solubility [22]. To solve this problem, some researchers use lipid excipient to carry insoluble drugs [23]; some use solid dispersions in soluble carriers to aid the transport of drugs [21, 24]; some use nanoparticles to improve bioavailability of the drugs [25, 26].



2.2.2 Targeted delivery of drugs

Most drugs are transported via the circulatory system, hence possible to affect every cell in the body, causing undesirable side effects. This is an especially important issue in cancer therapy. Targeted delivery aims to release the drugs precisely at specified targets with appropriate dosage and time, that is, controlled release.

The main strategy to controlled release is to develop stimuli-responsive materials as drug carriers. These “smart” materials have the characteristic that release of drugs will only be triggered by target-specific microenvironmental conditions, such as temperature, pH, pressure, light, ionic strength, or functional groups. Different kinds of systems such as polyelectrolyte multilayers [27-29], mesoporous silica nanoparticles [30-32], and block copolymers [33-35] have been used.

For cancer treatment, tumor microenvironment has been exploited for targeted delivery of drugs. Tumor cells have higher temperatures than normal body cells, so temperature-sensitive nanoparticles may be used to release the drug once arrived at tumor cells [36]. Also, tumor cells use glycolysis to obtain extra energy, causing a lower-pH environment [37]; pH-sensitive nanoparticles are suited in this situation.



2.3 Polymeric Nanoparticles

2.3.1 Hydrophobic Interaction

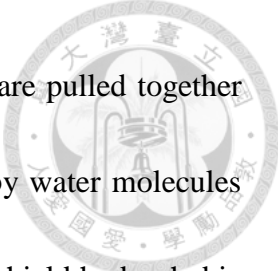
Hydrogen bonding plays an important role in aqueous systems. When solute molecules get into water, the water molecules will reorganize to solvate the solute molecules, and this involves breaking and formation of hydrogen bonding and also the creation of solvent-solute interface, depending on the polarity of the solute [38].

If the solute is nonpolar, then the introduction of solute molecule into water will reduce the number of hydrogen bonding between water molecules and produce an interface between water and solute molecules, the interfacial energy being approximately equal to that of water-vapor interface, so the solute molecule may be treated as a cavity in the aqueous solution [39]. The entropic and enthalpic changes on solvation determine the final configuration of the solutes in water.

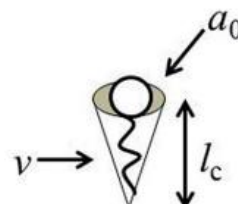
The effect of nonpolar solutes to reduce water-water hydrogen bonding is mainly entropic, and this makes solute-water interaction less favorable than water-water interaction, so the interaction between nonpolar solutes themselves tends to be stronger in aqueous environments. This is referred to as “hydrophobic interaction” [40].

2.3.2 Shapes of aggregation of Amphiphilic Molecules

Amphiphilic molecules, which have both hydrophobic and hydrophilic parts, tend



to aggregate in water. Hydrophobic parts of amphiphilic molecules are pulled together by the hydrophobic interaction, while hydrophilic parts are drawn by water molecules and tend to separate from each other, the overall effect being that to shield hydrophobic parts from water molecules by hydrophilic parts, and the surface formed by hydrophilic parts are stretched to attain minimum surface energy. The geometry of amphiphilic molecules determines the morphology of their aggregates. Israelachvili defined a dimensionless packing parameter and showed that different values of packing parameter lead to different shapes of aggregates, like spherical micelle, cylindrical micelle, bilayer, vesicle, and inverted micelle (Figure 2-1) [41, 42].



$$CPP = v/a_0 l_c$$


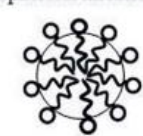

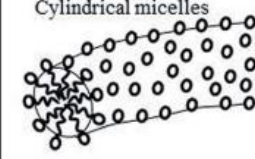



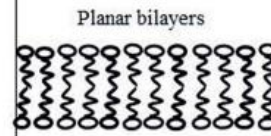

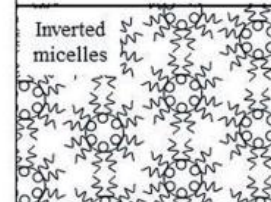
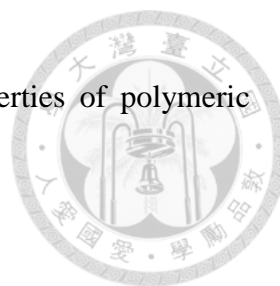
Critical Packing Parameter ($v/a_0 l_c$)	Critical Packing Shape	Structures Formed
$< 1/3$	 Cone	Spherical micelles 
$1/3 - 1/2$	 Truncated cone	Cylindrical micelles 
$1/2 - 1$	 Truncated cone	Flexible bilayers, vesicles 
~ 1	 Cylinder	Planar bilayers 
> 1	 Inverted truncated cone or wedge	Inverted micelles 

Figure 2-1 Relationship between critical packing parameter and shapes of aggregation of amphiphilic molecules

2.3.3 Amphiphilic Copolymers

Amphiphilic block and graft copolymers are commonly used to make nanoparticles. Like low-molecular-weight amphiphiles, they form spherical micelles, rod-like micelles, bilayers and vesicles (also called polymersomes). In addition, triblock copolymers can form core-shell spheres, Janus spheres, Janus cylinders, Janus vesicles, and many other structures [43]. By manipulating the length, the composition, and the



topology of the blocks, we can control the shape and other properties of polymeric nanoparticles.

2.3.4 Temperature-sensitive Copolymers as Carriers for Targeted

Delivery

Poly(N-isopropylacrylamide) (PNIPAAm) has been much studied for its temperature-dependent solubility in water. PNIPAAm exhibits a lower critical solution temperature (LCST) around 32°C. Below the LCST, PNIPAAm is soluble in water, but above the LCST, it becomes hydrophobic and is separated from water. This is due to the temperature-dependent strength of hydrogen bonding between PNIPAAm and water molecules [44]. The general phase diagram of a system exhibiting LCST is shown in Figure 2-2 [45]. In Figure 2-2, ϕ refers to polymer volume fraction, and T refers to temperature.

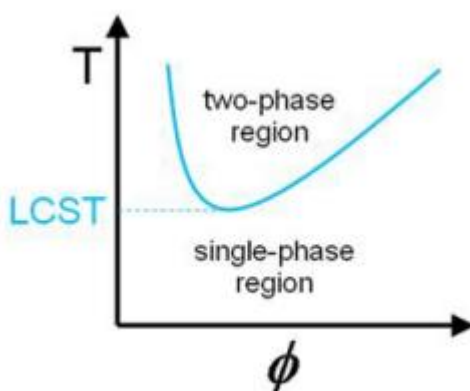



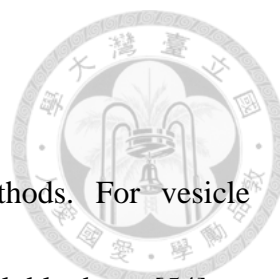
Figure 2-2 Phase diagram of a system exhibiting lower critical solution temperature



The temperature-dependent behavior of PNIPAAm has been utilized to make temperature-sensitive nanoparticles [46-49]. These nanoparticles are formed by copolymers which consist of one block of PNIPAAm, which is temperature-sensitive, and other blocks which are hydrophobic but not temperature-sensitive. They are amphiphilic below a certain temperature (the LCST), but become hydrophobic and insoluble above LCST. Below LCST, the amphiphilic nature of these copolymers leads to formation of self-assembled vesicles, micelles, and other shapes of nanoparticles; above LCST, they will phase-separate from water, and the nanoparticles will disassemble. The assembly and disassembly of temperature-responsive nanoparticles, which can be controlled by temperature variation, has been used in controlled release of drugs, particularly in cancer treatment.

There exists other polymers that exhibit LCST. For example, phase behavior and the influence of salts on poly(*N*-vinylpyrrolidone) and other pyrrolidone-based polymers have been studied [50, 51]. Copolymers based on poly(*N*-vinylcaprolactam) have been synthesized and characterized [52, 53].

LCST of polymers may be concentration-dependent. The LCST of the polymer PNIPAAm is relatively concentration-independent; other polymers exhibit concentration dependence, but the dependency is more significant in lower concentrations.



2.3.5 Drug loading and release

Drugs may be loaded into nanoparticles by various methods. For vesicle nanoparticles, one can use the nanoprecipitation method for water-soluble drugs [54], or use electrospraying for low aqueous solubility drugs [55]. Drugs may also be loaded simply by mixing the nanoparticle molecules with drugs [56-58]. Separation of unloaded drugs from drug-loaded nanoparticles can be achieved by centrifugation or dialysis.

Drug release profile varies according to the release mechanism of nanoparticles. For insoluble spherical nanoparticles, Higuchi proposed a model based on Fick's first law of diffusion [59]. For temperature-responsive nanoparticles, this model may be inappropriate. Most drug release experiments were done using dialysis, microfiltration or ultrafiltration to separate released drugs from nanoparticles [54-58].

To estimate the performance of nanoparticles in drug delivery, one can use the "drug entrapment" (also called "entrapment efficiency") defined as the ratio of the mass of drug entrapped in nanoparticles to the mass of total (free and entrapped) drug in solution [54, 60].

2.4 Poly(propylene glycol)

Poly(propylene glycol) (PPG), also called poly(propylene oxide) (PPO), is a

polyether (Figure 2-3). It is soluble in water below about 15°C and become less soluble in higher temperatures [61]. Shorter-chain PPGs has higher solubility in water than longer-chain PPGs [62]. That is, shorter-chain PPGs are more hydrophilic than longer-chain ones. Shorter-chain PPGs exhibit LCST, which is utilized as the temperature-responsive part of the material PPG-bis-adenine.

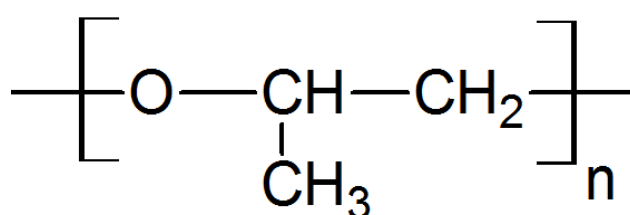


Figure 2-3 Structure of Poly(propylene glycol)

2.5 Nucleobases

The structures of the four nucleobases which occur in DNA are shown in Figure 2-5. The DNA double helices are stabilized by hydrogen bonding between the nucleobases (adenine, guanine, cytosine, and thymine) and π - π interaction between layers of nucleobases. The adenine-thymine and guanine-cytosine pairing by hydrogen bonding are especially strong, and this is the basis of storage of genetic information in DNA. Nevertheless, other modes of hydrogen bonding between nucleobases are possible, though less strong (Figure 2-4).

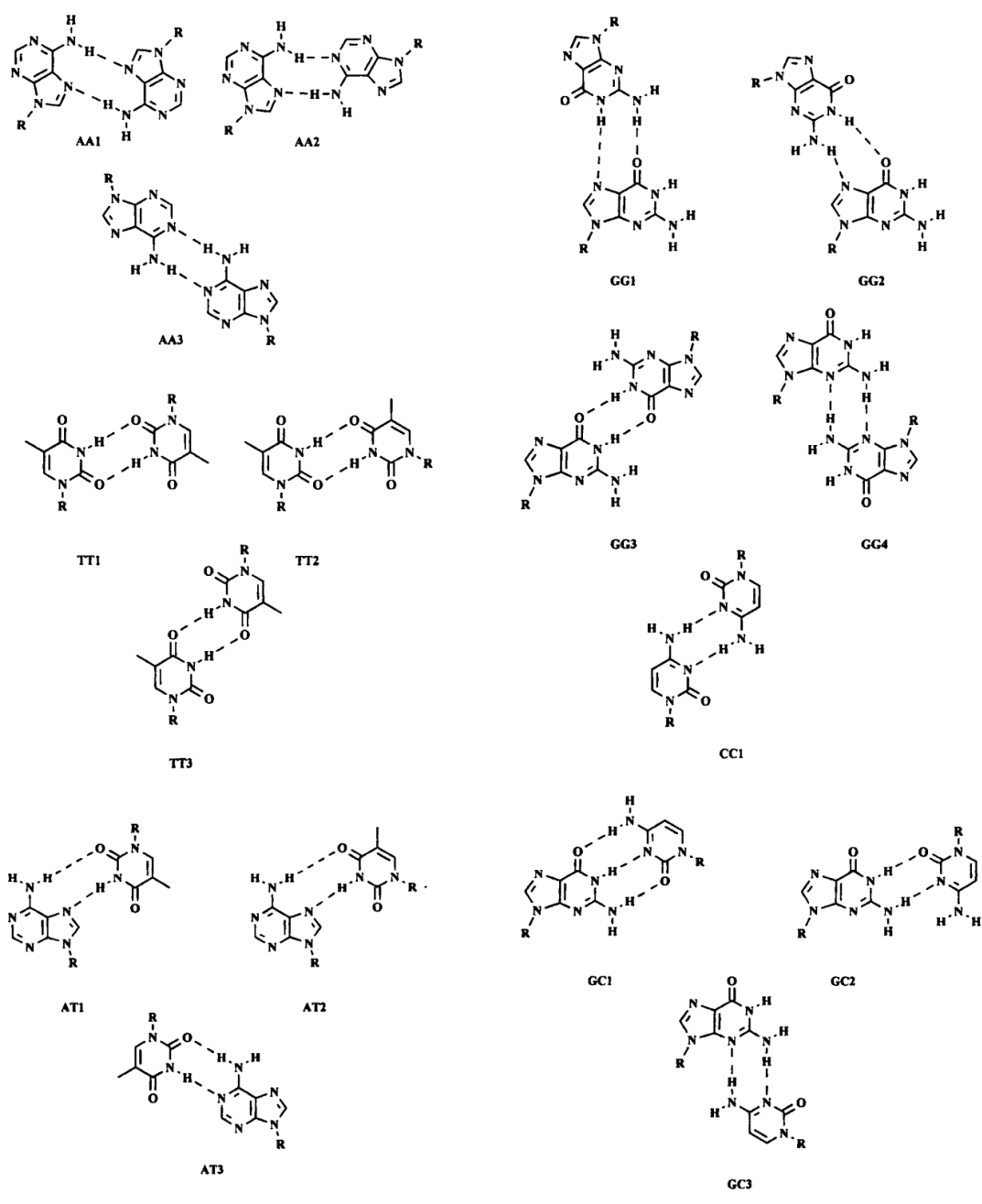


Figure 2-4 Various modes of hydrogen bonding between nucleobases

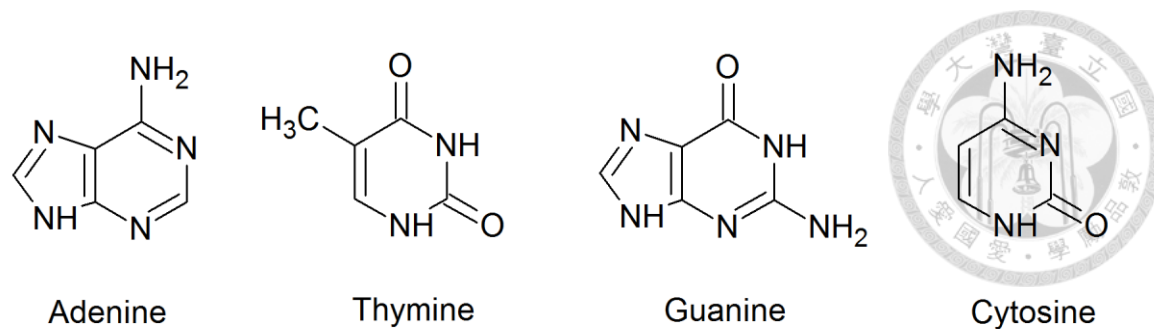


Figure 2-5 Structures of nucleobases which occur in DNA

Chapter 3. Materials and Methods

3.1 Synthesis of PPG-bis-adenine

3.1.1 The Addition Reaction

Poly(propylene glycol) 800 diacrylate (8.33 g), adenine (3.55 g), N,N-dimethylformamide (DMF) (120 mL), and potassium tert-butoxide (0.09 g) were added into a bottle, in that order. The mixture was stirred and kept at 70°C and allowed to react for 7 days. Small amount of potassium tert-butoxide (catalyst) were added every day to ensure complete conversion. The reaction for the synthesis was as shown in Figure 3-1, and its mechanism is analogous to the Michael addition.

After 7 days of reaction, DMF was removed from the bottle by vacuum distillation. The residue contains the product, Poly(Propylene glycol)-bis-adenine (PPG-bis-adenine), and unreacted adenine. 200 mL dichloromethane was added into the bottle to dissolve the residue. The solution was filtered, the filtrate collected, and the

filtrate was evaporated to get the product. The product was purified twice more by dissolution in dichloromethane followed by filtration and evaporation.

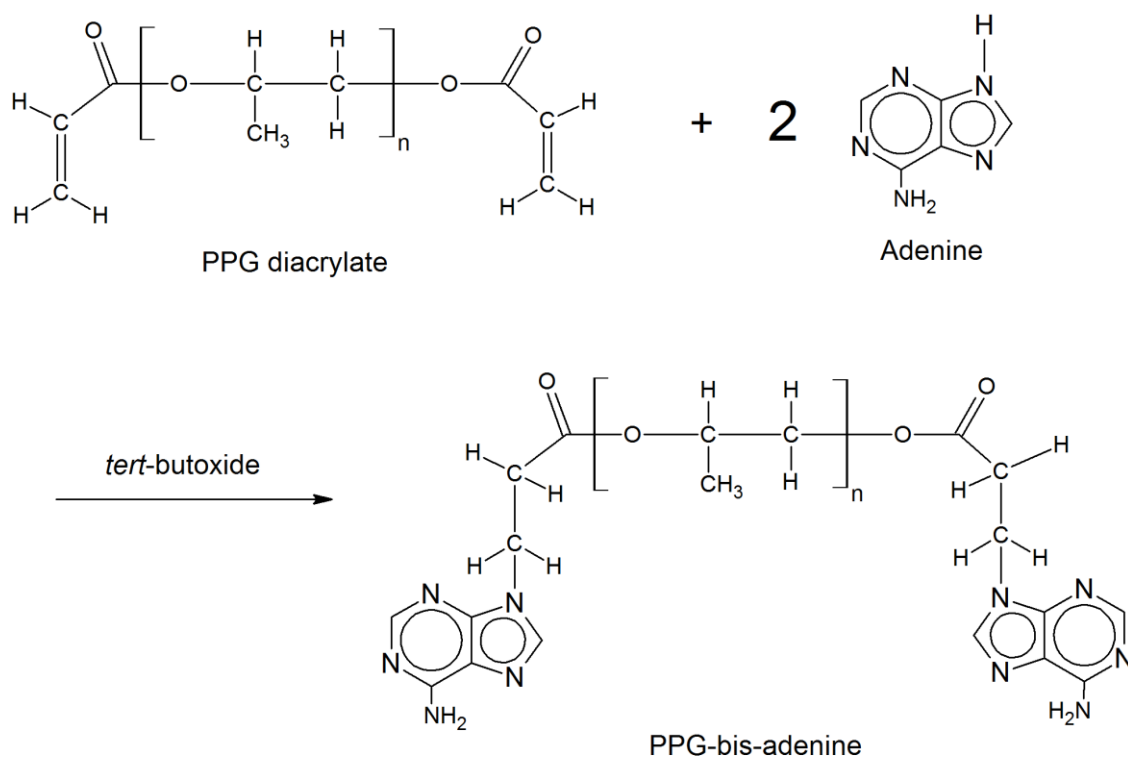
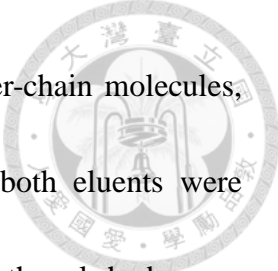


Figure 3-1 The reaction for the synthesis of PPG-bis-adenine

3.1.2 Purification by Column Chromatography

PPG hydrophilicity increases with decreased chain length, so only molecules with shorter PPG section have the desired temperature-responsive property. Column chromatography was employed as follows for the separation of shorter-chain molecules from longer-chain molecules. Silica gel was used as the adsorbent for column chromatography. Silica gel was packed into a column and was pre-loaded by n-hexane.



PPG-bis-adenine was firstly eluted by dichloromethane to get longer-chain molecules, and then by methanol to wash the shorter-chain molecules out, both eluents were collected. After rotary evaporation, only the part eluted by methanol had some yellowish solid left in the bottle. The solid was collected and washed by diethyl ether twice and stored for subsequent use.

3.2 Nuclear Magnetic Resonance (NMR)

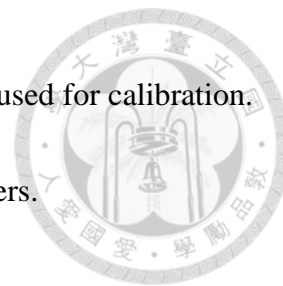
^1H NMR was taken by Bruker Avance DMX 500MHz FT-NMR at room temperature. The sample was prepared as follows. 45 mg of solid PPG-bis-adenine was filled into an NMR tube, and CDCl_3 was added to dissolve the solid. After dissolution of PPG-bis-adenine, CDCl_3 was added to the height of 4 cm (the total volume of CDCl_3 used was about 0.8 mL). Peak and integration analysis of the spectrum was done using ACD/NMR Processor.

3.3 Gel Permeation Chromatography (GPC)

GPC of PPG-bis-adenine and PPG 800 diacrylate were performed on Waters system, with the temperature set at 35°C . Samples were dissolved in tetrahydrofuran (THF), the concentration being 2 mg/mL for both PPG-bis-adenine and PPG 800 diacrylate. The mobile phase for GPC was THF. Samples were filtered through $0.20\text{-}\mu\text{m}$ hydrophilic PTFE filters before injection. The elution time was 40 minutes. Polystyrene

with molecular weights 387000, 43700, 6520, and 1010 g/mol were used for calibration.

Analysis was performed on Empower Pro software provided by Waters.



3.4 Elemental Analysis

Elemental analysis was performed on an Elementar Vario EL cube. This instrument was for N, C, S, and H analysis. 2-3 mg of PPG 800 diacrylate and PPG-bis-adenine, respectively, were used as sample. The precision of the instrument is $\pm 0.2\%$. Samples were oxidized to form nitrogen oxides, water, carbon dioxide, and sulfur dioxide, followed by reduction of nitrogen oxides to nitrogen gas, and separation of the gases produced in the instrument. The detector then detected the weight percentages of nitrogen, hydrogen, carbon, and sulfur. The whole reaction process and analysis were controlled by computer.

3.5 Mass Spectroscopy (MALDI-TOF-TOF)

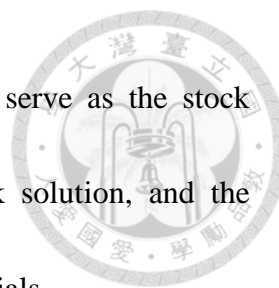
MALDI-TOF-TOF of PPG-bis-adenine and PPG 800 diacrylate were performed on a Bruker system. The matrix used was 2,5-dihydroxybenzoic acid (DHB) for both samples. The matrix was ionized first in the instrument, then the charge was transferred to the sample. The indirect charge transfer reduces the rate of decomposition of polymeric samples. The sample flew through a magnetic field, and each molecule in the sample was separated according to its mass-to-charge ratio. The detector then detected

the relative intensity of each mass-to-charge value, and the result was outputted to a computer.



3.6 Critical Micelle Concentration (CMC) determination by pyrene fluorescence

Pyrene is a non-polar compound, and its fluorescence is sensitive to the environment it experiences. The spectra of pyrene fluorescence are different in different solvents. This difference is prominent between non-polar and polar solvents. In particular, the ratio of emission intensity of the third peak to that of the first peak (“peak III to peak I ratio”) between 360 nm and 400 nm under 339-nm excitation is larger in less polar solvents [63-65]. This behavior has been utilized in determination of CMC of surfactants [66, 67]. Because the structure of aggregation is not clear yet, it is better to call “critical aggregation concentration”, but we will use the more common term “critical micelle concentration” whether the nanoparticles are micelles or not. When there is no micelle (or other forms of aggregation) in the solution, pyrene experiences an aqueous environment, and the vibronic fine structure of its fluorescent emission spectra reveals polar characteristics. When the concentration of PPG-bis-adenine is above CMC, pyrene would move into non-polar area of the micelles (or other forms of aggregation), and the vibronic fine structure of its spectra shows non-polar characteristics.




Pyrene (3.6×10^{-3} g) was dissolved in 20 mL acetone to serve as the stock solution. To each of 10 vials was added 40 μ L of pyrene stock solution, and the solutions were allowed to evaporate, leaving solid pyrene in the 10 vials.

Table 3-1 Sample Concentrations for CMC determination

No. of sample	Concentration (mg/mL)
1	$10^{0.0}$
2	$10^{-0.5}$
3	$10^{-1.0}$
4	$10^{-1.5}$
5	$10^{-2.0}$
6	$10^{-2.5}$
7	$10^{-3.0}$
8	$10^{-3.5}$
9	$10^{-4.0}$
10	$10^{-4.5}$

Table 3-1 shows the concentrations of the samples used in the determination of CMC. The samples were prepared as follows. Firstly, 13.1 mg of PPG-bis-adenine was



dissolved in 13.1 mL DI water to get sample no. 1. Sample no. 1 was diluted by DI water to get sample no. 2. Samples no. 3, 5, 7, and 9 were obtained by successive dilution from sample no. 1. Similarly, samples no. 4, 6, 8, and 10 were obtained by successive dilution from sample no. 2.


Pyrene fluorescence spectra were recorded by a Cary Eclipse Varian fluorescence spectrophotometer. The excitation wavelength was 339 nm, and emission spectra between 363.50 nm and 400.00 nm were recorded, the data interval was 0.5 nm. Excitation slit of 10 nm and emission slit of 2.5 nm were used, and the photomultiplier tube voltage was set to 680 V. Savitzky-Golay smoothing was employed to smooth the data. The filter size of Savitzky-Golay was 5.

The “peak III to peak I” ratio was plotted against the logarithm of concentration of PPG-bis-adenine solution. The CMC was determined to be the point from which the ratio begins to increase.

3.7 Lower Critical Solution Temperature (LCST) determination by UV/Visible spectrophotometry

Aqueous solution of PPG-bis-adenine exhibits LCST. Below LCST, the solution is transparent, but it becomes cloudy above LCST (Figure 3-2). This corresponds to the change in transmittance of light. With a preliminary scan, we chose the wavelength with

highest transmittance below LCST as the basis of measurement, which is at 800 nm.



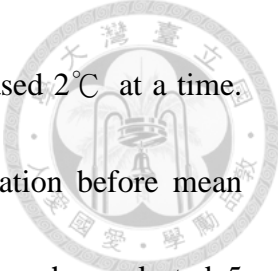
5 mg/mL of PPG-bis-adenine DI-water solution was prepared, and successively diluted by DI water to obtain 4, 3, 2, and 1 mg/mL solutions. Samples were filtered through 0.45- μ m hydrophilic PTFE filters before measurement. Transmittances of 800 nm light at different temperatures were recorded using a Jasco V-650 spectrophotometer. For each concentration, the measurement temperature was fixed at a level well below LCST, then the temperature was increased 2 $^{\circ}$ C at a time and the transmittance of the sample was measured at the new temperature. Each sample was equilibrated for 2 minutes before measurement after the temperature was changed. The temperature was increased until the transmittance goes to almost zero and does not change very much with temperature. LCST was determined as the temperature at which transmittance equals 50%.



Figure 3-2 Color of solution below (left) and above (right) LCST

3.8 Mean diameter measurement by Dynamic Light Scattering (DLS)

5 mg/mL of PPG-bis-adenine DI-water solution was prepared, and successively diluted by DI water to obtain 4, 3, 2, and 1 mg/mL solutions. The mean diameters of nanoparticles of each concentration were measured using a Malvern Zetasizer Nano ZS. Each sample was filtered through a 0.45- μm hydrophilic PTFE filter before measurement. For each concentration, measurements were taken at various temperatures,



from well below LCST to above LCST. The temperature was increased 2°C at a time. After each temperature variation, there was a 10 minutes equilibration before mean diameter measurement. For each measurement, there were 8 runs, each run lasted 5 seconds. The mean and standard deviation of each measurement were obtained using the best 4 runs (in terms of quality automatically judged by the Zetasizer software) determined by the computer software.

3.9 Zeta potential measurement

DI-water solution of PPG-bis-adenine with concentration 5 mg/mL was prepared. The solution was diluted by DI water to obtain 4, 3, 2, and 1 mg/mL solutions. All five samples were filtered through 0.45- μm hydrophilic PTFE filters. Samples were measured using a Malvern Zetasizer Nano ZS with attenuator set to 10. Each sample was measured 5 times, each time with 12~20 runs. Each run lasted 3 seconds. The best 50% runs (in terms of quality automatically judged by the Zetasizer software) were chosen as valid data for mean and standard deviation calculation.

3.10 Scanning Electron Microscopy (SEM)

1 mg/mL of PPG-bis-adenine DI-water solution was prepared, and then successively diluted by DI water to obtain 0.1, 0.01, and 0.001 mg/mL solutions. Each sample was dropped onto a 1 cm \times 1 cm silicon wafer, then spin-coated for 1 minute

at 4000 rpm. The spin-coated wafers were dried in vacuum for 24 hours. Platinum was sputtered onto the samples by a sputtering system for 10 minutes before SEM observation.



The SEM images were taken by FEI company's Nova NanoSEM 230 system.

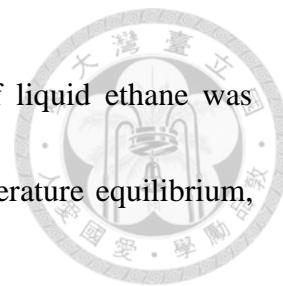
3.11 Cryogenic Transmission Electron Microscopy (cryo-TEM)

Cryogenic transmission electron microscopy (cryo-TEM) is a technique that can retain the aqueous environment of samples by instant freezing.

1 mg/mL DI-water solution of PPG-bis-adenine was prepared and filtered through a 0.45- μ m hydrophilic PTFE filter to serve as the sample. Copper grid with a layer of carbon covered on it was used to hold the sample solution. There was an array of holes on the carbon film (this is called a holey carbon film).

The sample preparation was done by a machine with the following procedure. The copper grid was placed in a chamber with 100% relative humidity to prevent evaporation of solution nanofilm (see below) on the copper grid. One droplet of sample solution was transferred onto the grid under room temperature, then pressed by a filter paper to remove most of the solution, leaving only a hundred-nanometer-thin film of solution on the grid. Then the copper grid was plunged into liquid ethane to instantly freeze the solution nanofilm.

The sample was kept in liquid ethane, and the container of liquid ethane was cooled by liquid nitrogen. The sample was kept one day for temperature equilibrium, and then transferred to the chamber of TEM for observation.

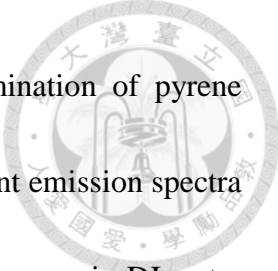


3.12 Drug Loading and Release

Pyrene was used as the model drug for loading and release experiment. 40 μL of Pyrene stock solution (1.8×10^{-4} g/mL acetone) was added into a vial, and acetone was allowed to evaporate, leaving solid pyrene in the vial. 10 mL of 3 mg/mL PPG-bis-adenine DI-water solution was added into the vial so that the final concentration of pyrene was 7.2×10^{-4} mg/mL. This concentration of pyrene will be referred to as 6 \times concentration in drug loading and release experiment of this study (so that 1 \times concentration = 1.2×10^{-4} mg/mL). Two methods of loading were compared:

1. The above-mentioned 6 \times pyrene solution was kept at 20 $^{\circ}\text{C}$ (which is under the LCST of 3 mg/mL PPG-bis-adenine solution, 38 $^{\circ}\text{C}$) for 24 hours.
2. The above-mentioned 6 \times pyrene solution was raised to 90 $^{\circ}\text{C}$ for 30 minutes, then cooled down under room temperature to 20 $^{\circ}\text{C}$ for 24 hours.

After drug loading, the solutions for both methods of loading were ultracentrifuged under 90000 rpm (average g-force 502135) for 30 minutes. The



supernatant (containing unloaded pyrene) was sampled for determination of pyrene concentration. The intensity of the first peak (at 373 nm) of fluorescent emission spectra under 339-nm excitation was used to calibrate the concentration of pyrene in DI-water solution containing 3 mg/mL PPG-bis-adenine.

For drug release experiment, the intensity of the first peak (at 373 nm) of fluorescent emission spectra under 339-nm excitation was used as an indicator of concentration variation. 6× pyrene in DI-water solution containing 3 mg/mL PPG-bis-adenine was prepared as in the loading experiment, and pyrene was loaded into PPG-bis-adenine nanoparticles using the first method in the loading experiment (temperature kept under LCST). The initial fluorescent emission intensity at 20°C was recorded. The solution was then heated to 50 °C (above LCST), causing the nanoparticles to disassemble and release pyrene. After heating, the solution was cooled down under room temperature. During the cooling process, the temperature crossed LCST again, and the nanoparticles reassembled and reloaded pyrene. The emission intensity was recorded every 4 seconds during the cooling process.

The fluorescent emission intensity was measured using Cary Eclipse Varian fluorescence spectrophotometer as in the CMC determination experiment.

Chapter 4. Results and Discussion



4.1 Structure Characterization

4.1.1 NMR Spectroscopy

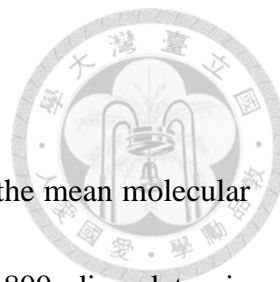
The ^1H NMR of PPG-bis-adenine is shown in Figure 4-1. Each class of hydrogen in the molecular structure was labelled in the figure, and the corresponding peaks in the spectra were indicated. The peaks in the spectra and the molecular structure are in good correspondence. The integration values of the peaks agree with the relative abundance of each class of hydrogen in the structure, indicating that the sample has the desired structure.

4.1.2 Mass spectroscopy & GPC

The theoretical molecular weight of PPG 800 diacrylate (the reactant) and PPG-bis-adenine (the product) of various degrees of polymerization are shown in Table 4-1. Due to some fragmentation, the dominant peaks in the spectrum do not correspond to the mass of the whole molecules. Rather, most of the peaks correspond to molecular weight after removal of two water molecules. Comparison of the MALDI-TOF mass spectrum of the reactant (PPG 800 diacrylate) and purified product (PPG-bis-adenine) (Figure 4-2) reveals that the average degree of polymerization of PPG decreased from

12 to about 7 after product purification.

From the data obtained by GPC (Figure 4-3), we can see that the mean molecular weight of purified PPG-bis-adenine is less than that of PPG 800 diacrylate, in agreement with the result of mass spectroscopy. The polydispersity of PPG-bis-adenine is seen to be less than that of PPG 800 diacrylate, indicating that the purity of the product was increased after the purification process.



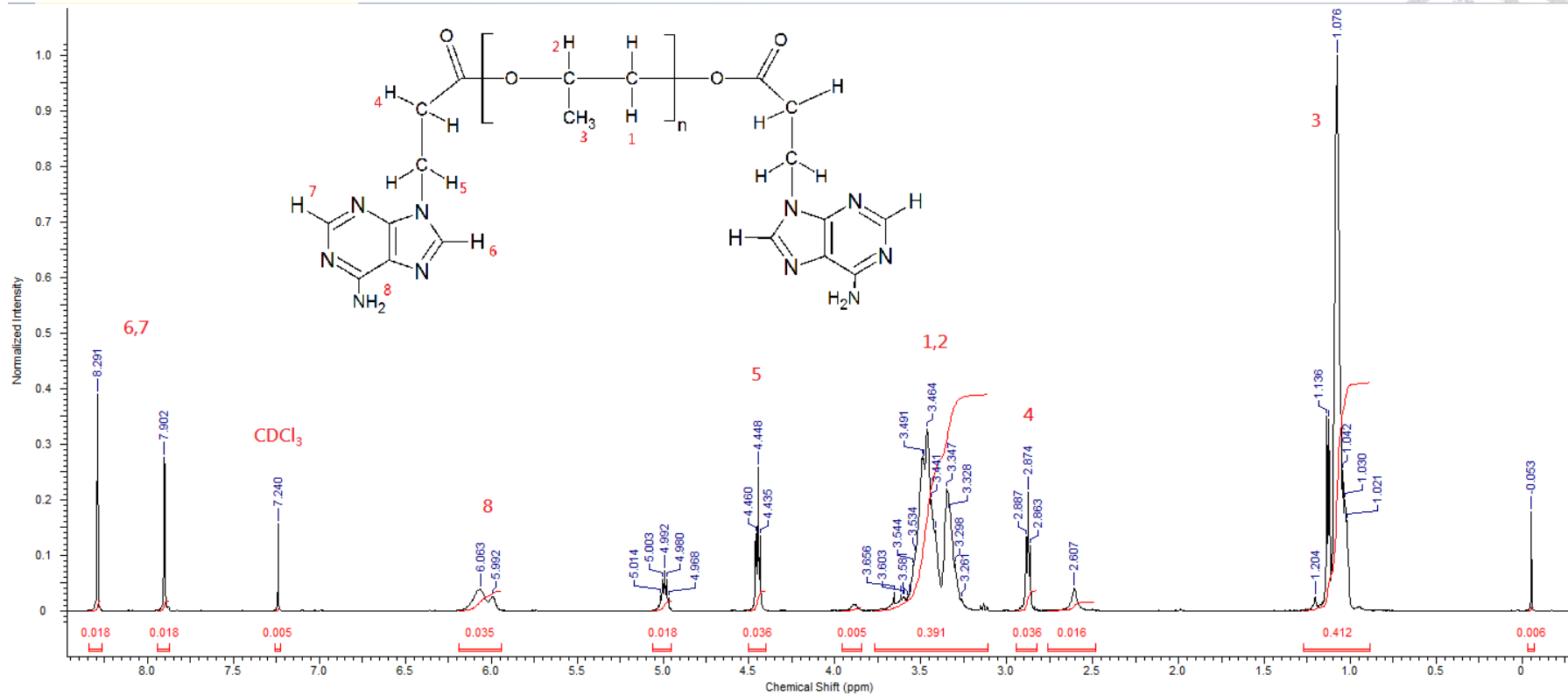


Figure 4-1 ^1H NMR spectroscopy of PPG-bis-adenine in CDCl_3

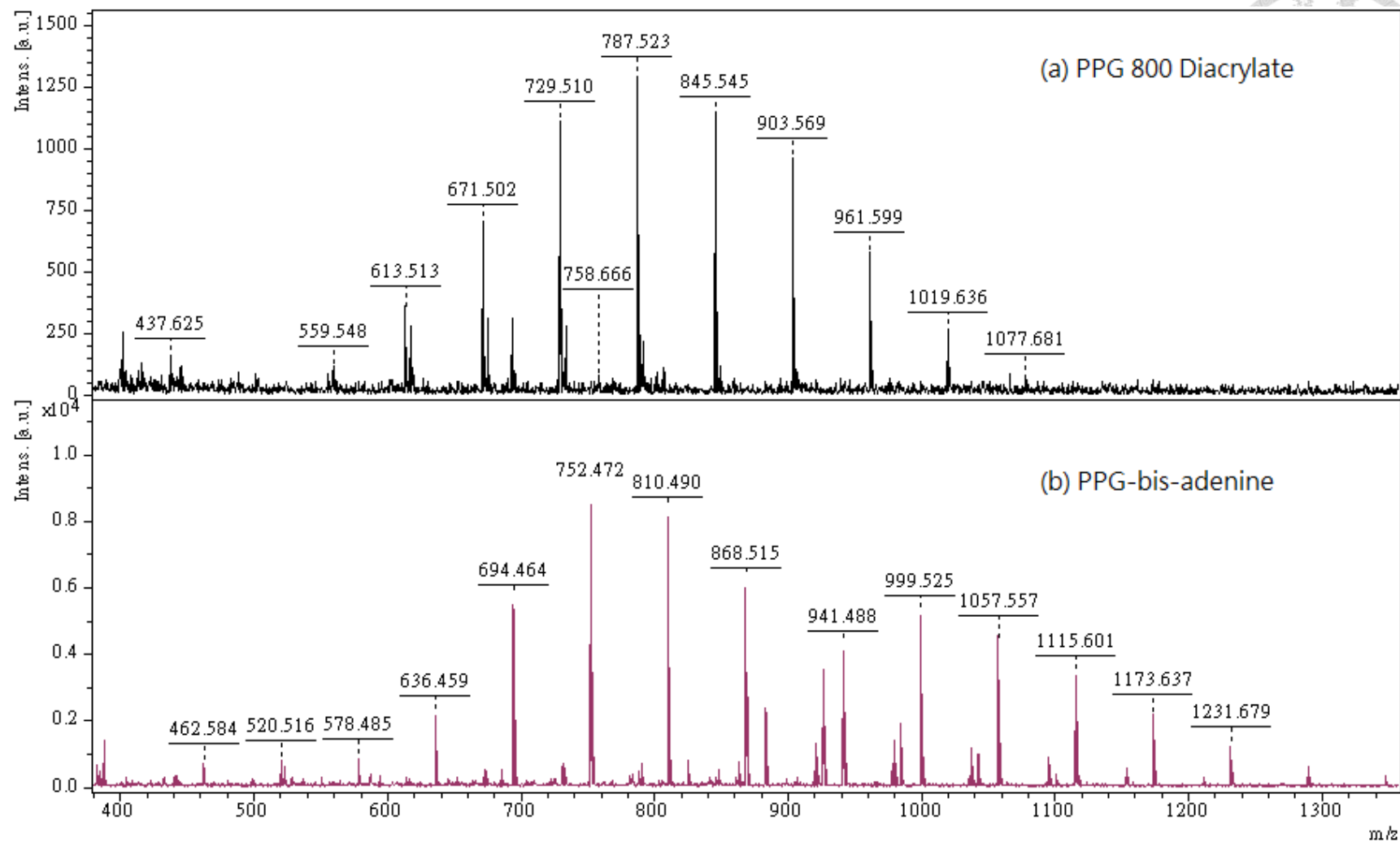


Figure 4-2 Mass spectrum of (a) PPG 800 diacrylate (reactant) and (b) PPG-bis-adenine (product)

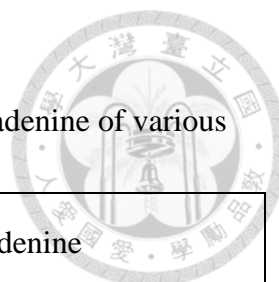
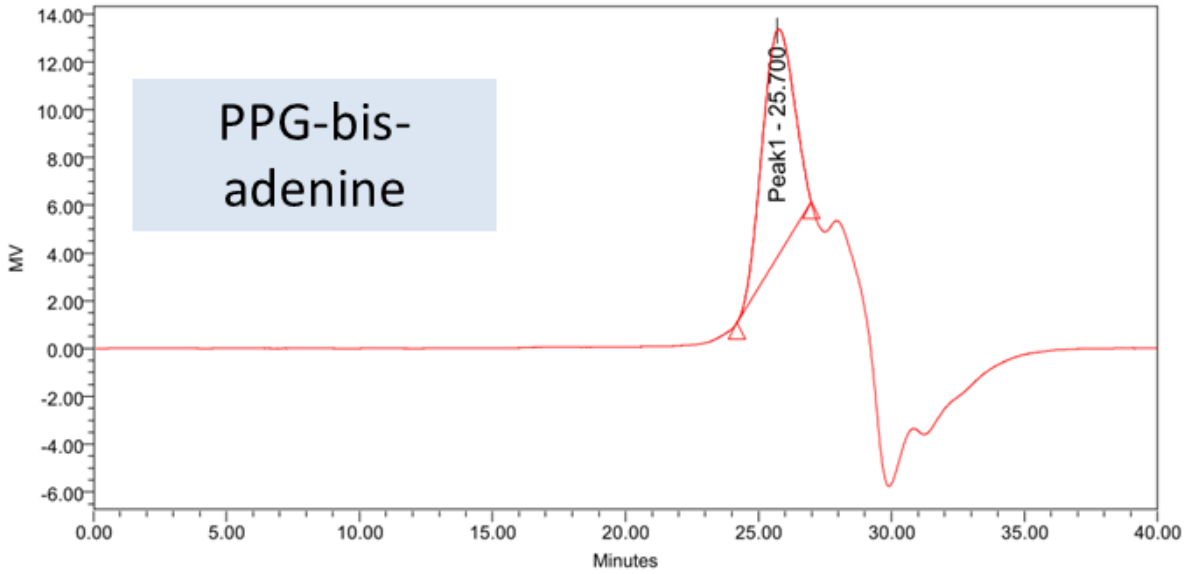
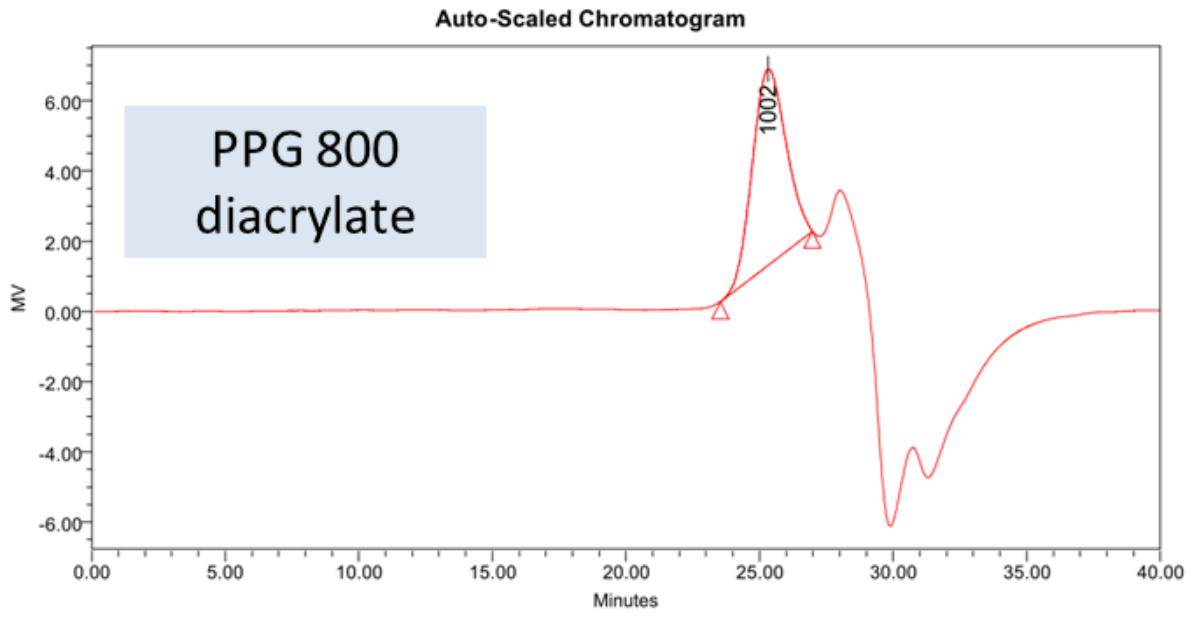


Table 4-1 Molecular weight of PPG 800 diacrylate and PPG-bis-adenine of various degrees of polymerization

PPG 800 diacrylate			PPG-bis-adenine		
Degree of polymerization	Molecular Weight (g/mol)	Minus 2*H ₂ O (g/mol)	Degree of polymerization	Molecular weight (g/mol)	Minus 2*H ₂ O (g/mol)
1	184.186	148.665	1	454.466	418.945
2	242.264	206.743	2	512.544	477.023
3	300.342	264.821	3	570.622	535.101
4	358.420	322.899	4	628.700	593.179
5	416.498	380.977	5	686.778	651.257
6	474.576	439.055	6	744.856	709.335
7	532.654	497.133	7	802.934	767.413
8	590.732	555.211	8	861.012	825.491
9	648.810	613.289	9	919.090	883.569
10	706.888	671.367	10	977.168	941.647
11	764.966	729.445	11	1035.246	999.725
12	823.044	787.523	12	1093.324	1057.803
13	881.122	845.601	13	1151.402	1115.881
14	939.200	903.679	14	1209.480	1173.959
15	997.278	961.757	15	1267.558	1232.037
16	1055.356	1019.835	16	1325.636	1290.115
17	1113.434	1077.913	17	1383.714	1348.193
18	1171.512	1135.991	18	1441.792	1406.271
19	1229.590	1194.069	19	1499.870	1464.349



GPC Results

	Dist Name	Mn	Mw	MP	Mz	Mz+1	Mv	Polydispersity	MW Marker 1	MW Marker 2
PPG 800 diacrylate	1	1197	1248	1002	1309	1381		1.042671		

GPC Results

	Dist Name	Mn	Mw	MP	Mz	Mz+1	Mv	Polydispersity	MW Marker 1	MW Marker 2
PPG-bis-adenine	1	1096	1119		1147	1177		1.021745		

Figure 4-3 GPC chromatogram of PPG 800 diacrylate and PPG-bis-adenine



4.1.3 Elemental analysis

The molecular formula of PPG diacrylate is $C_{3n+6}H_{6n+6}O_{n+3}$, and the molecular formula of PPG-bis-adenine is $C_{3n+16}H_{6n+16}O_{n+3}N_{10}$, where n is the number of monomer units of PPG. Theoretical atomic compositions are shown in Table 4-2, where n stands for the degree of polymerization. Figure 4-4 shows the composition of carbon and hydrogen of PPG diacrylate as a function of degree of polymerization, calculated from the formulas in Table 4-2. Figure 4-5 shows the composition of carbon and hydrogen of PPG-bis-adenine as a function of degree of polymerization, also calculated from the formulas in Table 4-2.

The result of elemental analysis is shown in Table 4-3. The compositions of carbon, hydrogen, and nitrogen are quite consistent with theoretical calculations, considering the error that may be caused by incomplete reaction of the samples.

Table 4-2 Theoretical atomic compositions of the reactant and the product

	C	H	O	N
PPG diacrylate	$\frac{(3n + 6) \cdot 12.01}{58.078n + 126.108}$	$\frac{(6n + 6) \cdot 1.008}{58.078n + 126.108}$	$\frac{(n + 3) \cdot 16.00}{58.078n + 126.108}$	0
PPG-bis-adenine	$\frac{(3n + 16) \cdot 12.01}{58.078n + 396.388}$	$\frac{(6n + 16) \cdot 1.008}{58.078n + 396.388}$	$\frac{(n + 3) \cdot 16.00}{58.078n + 396.388}$	$\frac{10 \cdot 14.01}{58.078n + 396.388}$

Table 4-3 Elemental analysis of the reactant and the product

	N (%)	C (%)	H (%)
PPG 800 diacrylate	0.109667	62.52833	8.826667
PPG-bis-adenine	11.698	57.061	7.907333

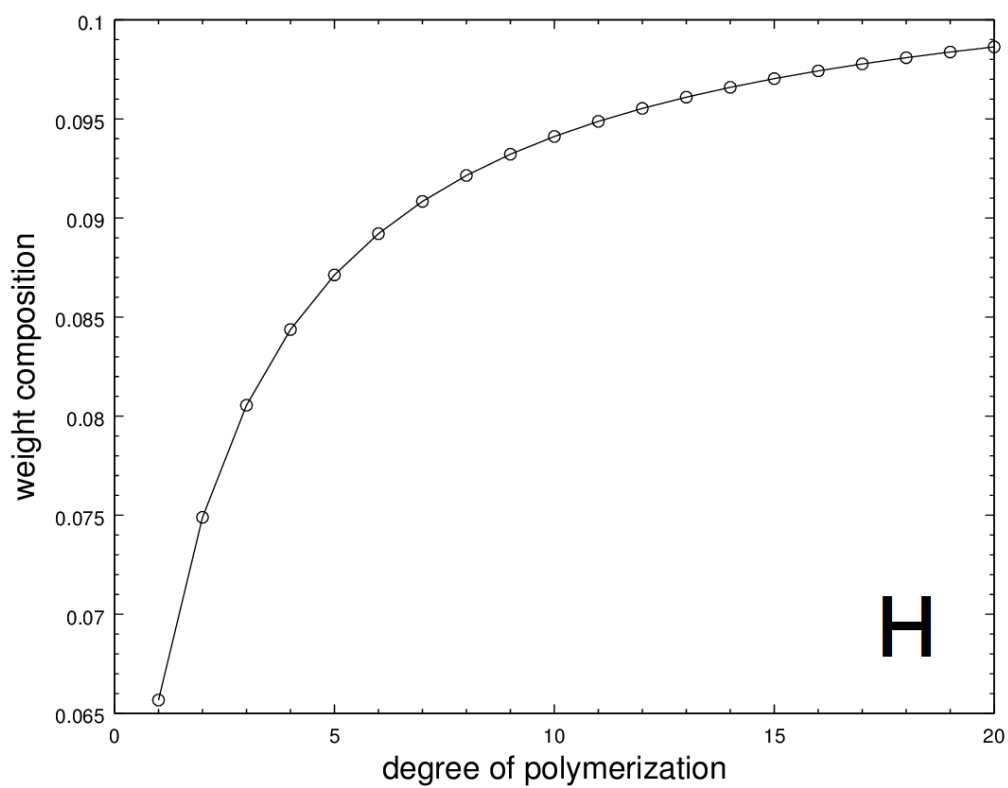
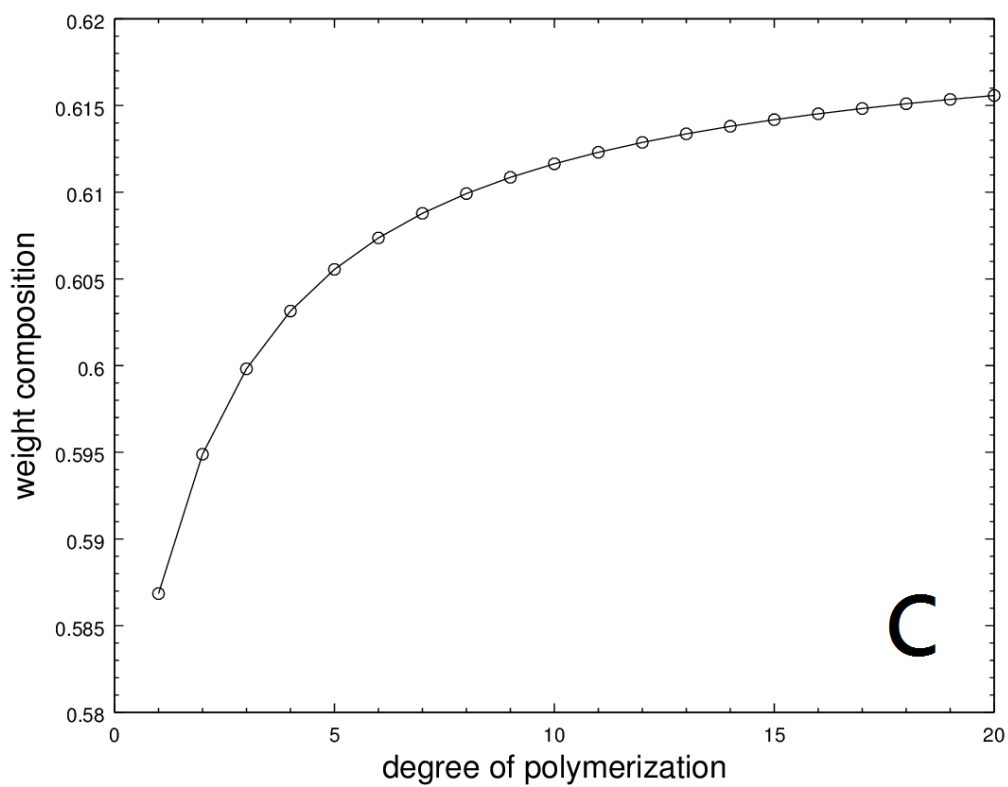


Figure 4-4 Theoretical carbon and hydrogen composition of PPG diacrylate as a function of degree of polymerization

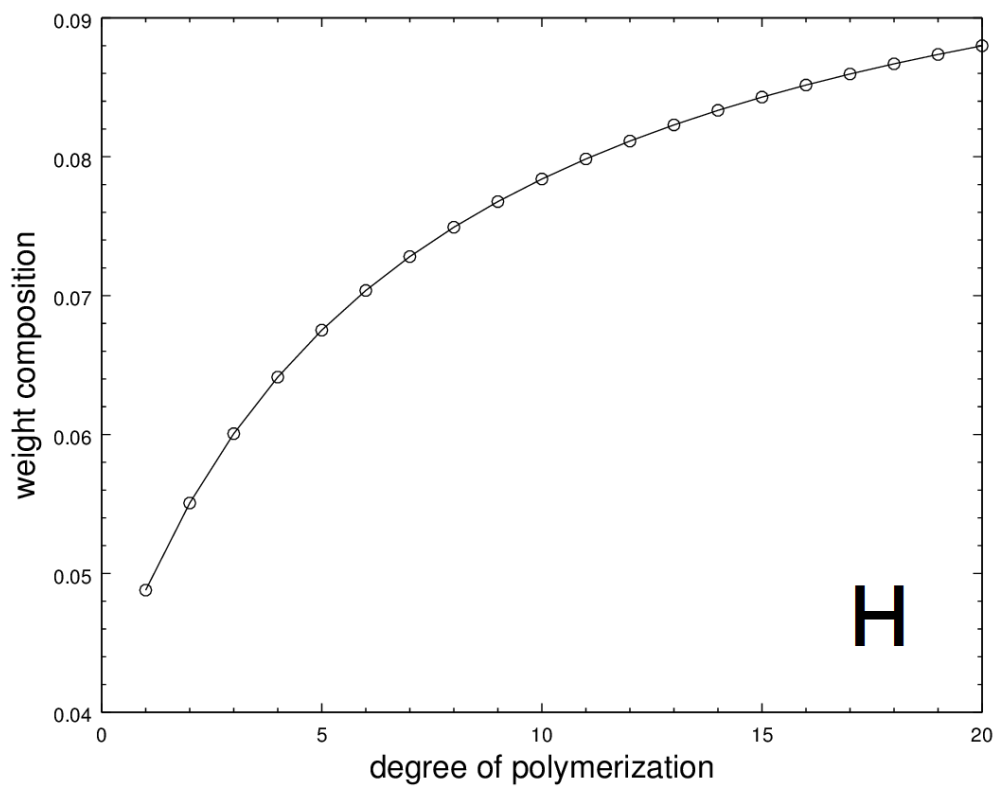
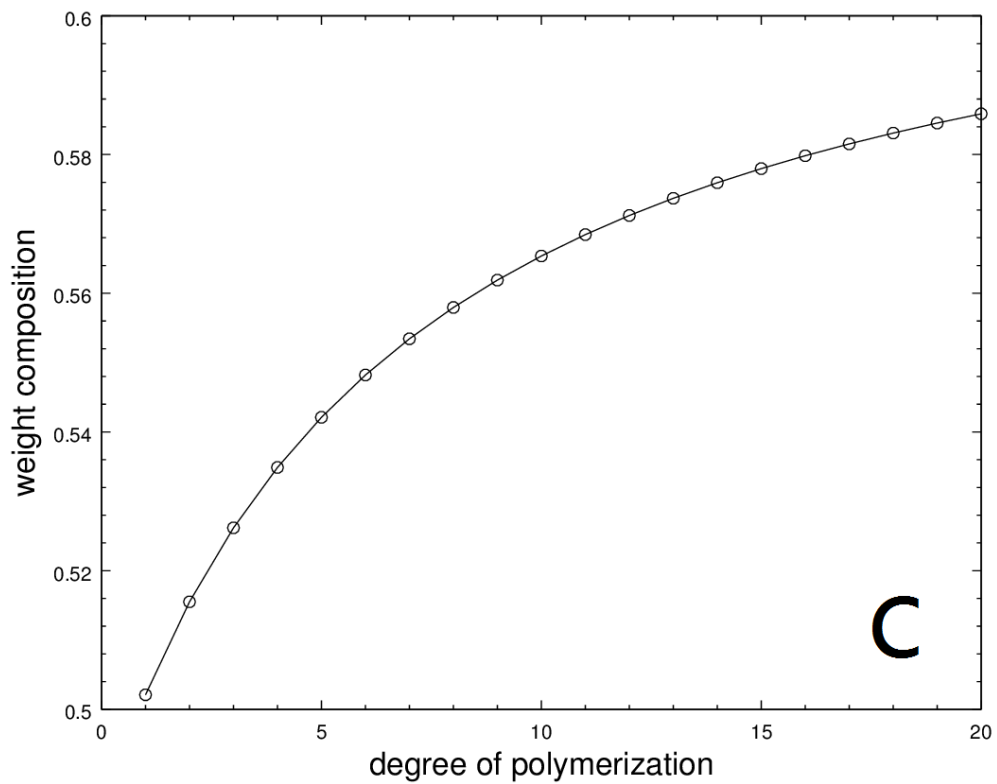


Figure 4-5 Theoretical carbon and hydrogen composition of PPG diacrylate as a function of degree of polymerization



4.2 Evidence of Nanoparticles

4.2.1 Dynamic light scattering

Temperature variation of mean diameter of PPG-bis-adenine nanoparticles for 1, 2, 3, 4, and 5 mg/mL solutions are shown in Figure 4-6 to Figure 4-10, respectively. Note that there is a marked change of mean diameter with temperature for each concentration. This change corresponds to the phase change around LCST. Below LCST, the mean diameter of PPG-bis-adenine nanoparticles is seen to be around 100 nm for all 5 concentrations, and does not change very much with temperature.

4.2.2 Scanning Electron Microscopy

The SEM image of 1 mg/mL and 0.1 mg/mL PPG-bis-adenine aqueous solution is shown in Figure 4-11 and Figure 4-12, respectively. The larger particles are aggregations of several smaller particles, while the smaller ones should be single particles. The nanoparticles are seen to be roughly spherical but irregular. The diameter of the smaller particles is about 30 nm, which is smaller than the mean diameter measured by DLS. This is because the sample of SEM was dried before observation. The drying process caused the nanoparticles to shrink. For 0.01 and 0.001 mg/mL solutions, nanoparticles were not found. This indicates non-existence or very low nanoparticle density under these concentrations.

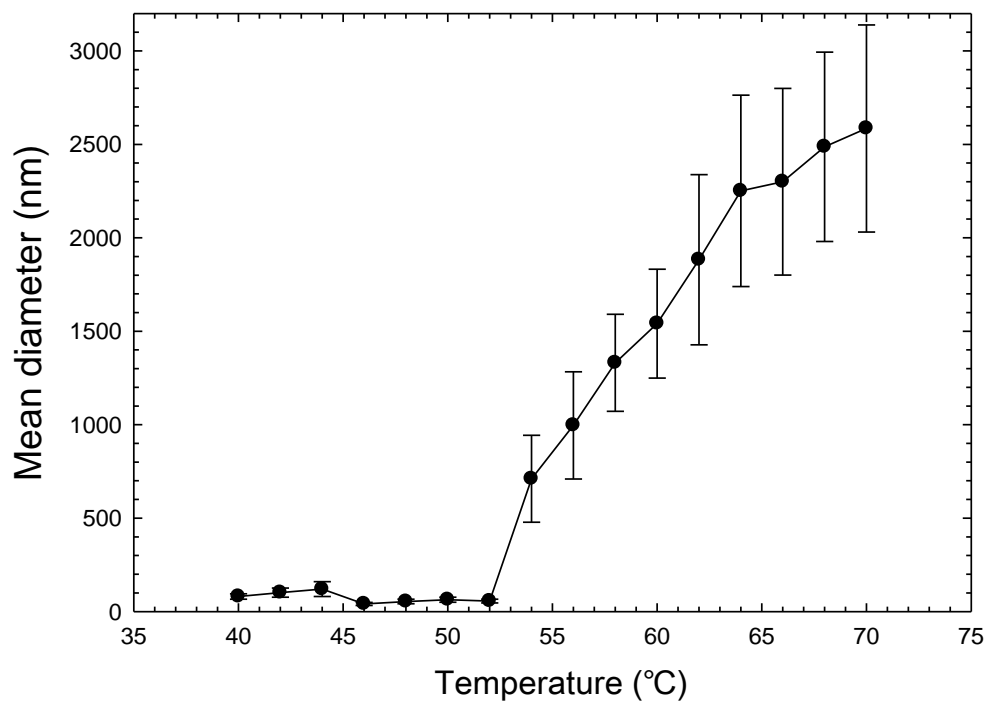


Figure 4-6 Variation of mean diameter of PPG-bis-adenine nanoparticles with temperature under 1 mg/mL

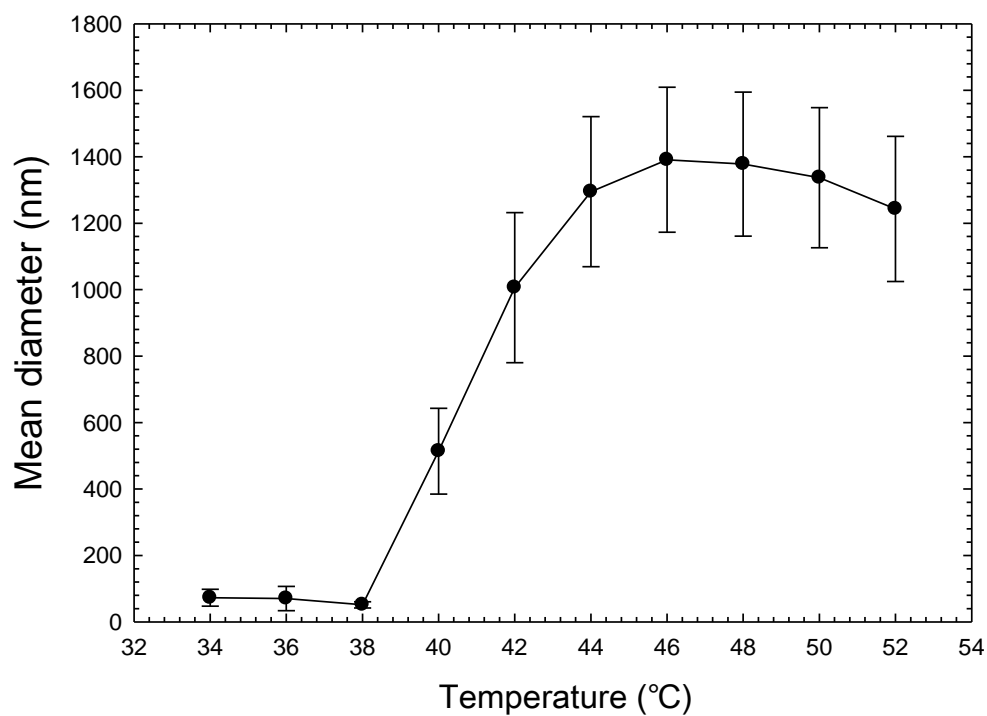


Figure 4-7 Variation of mean diameter of PPG-bis-adenine nanoparticles with temperature under 2 mg/mL

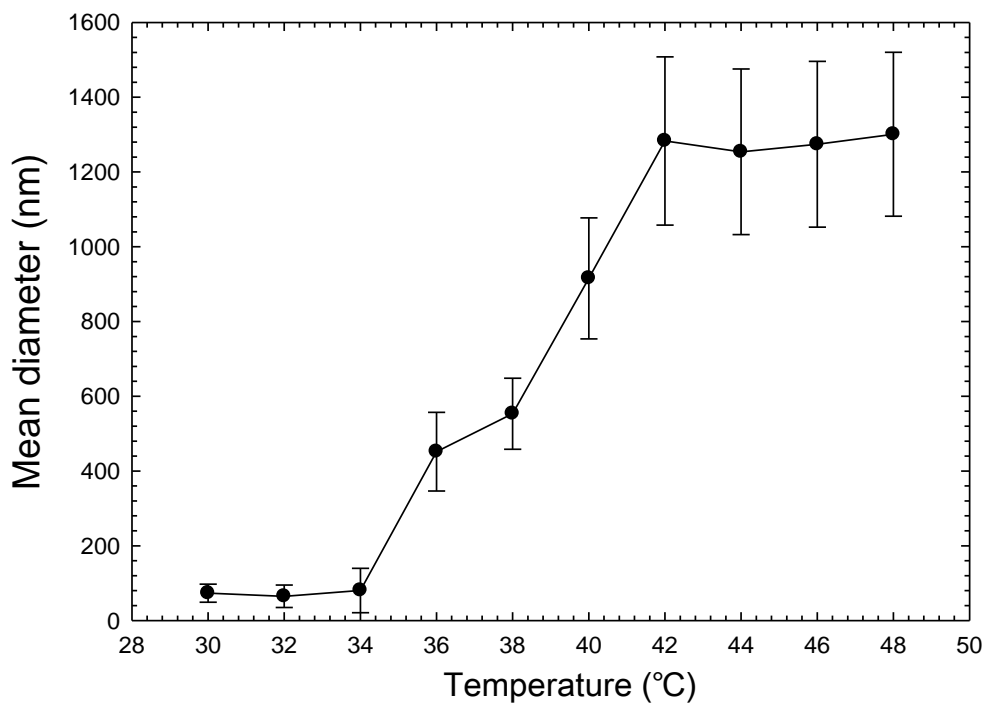


Figure 4-8 Variation of mean diameter of PPG-bis-adenine nanoparticles with temperature under 3 mg/mL

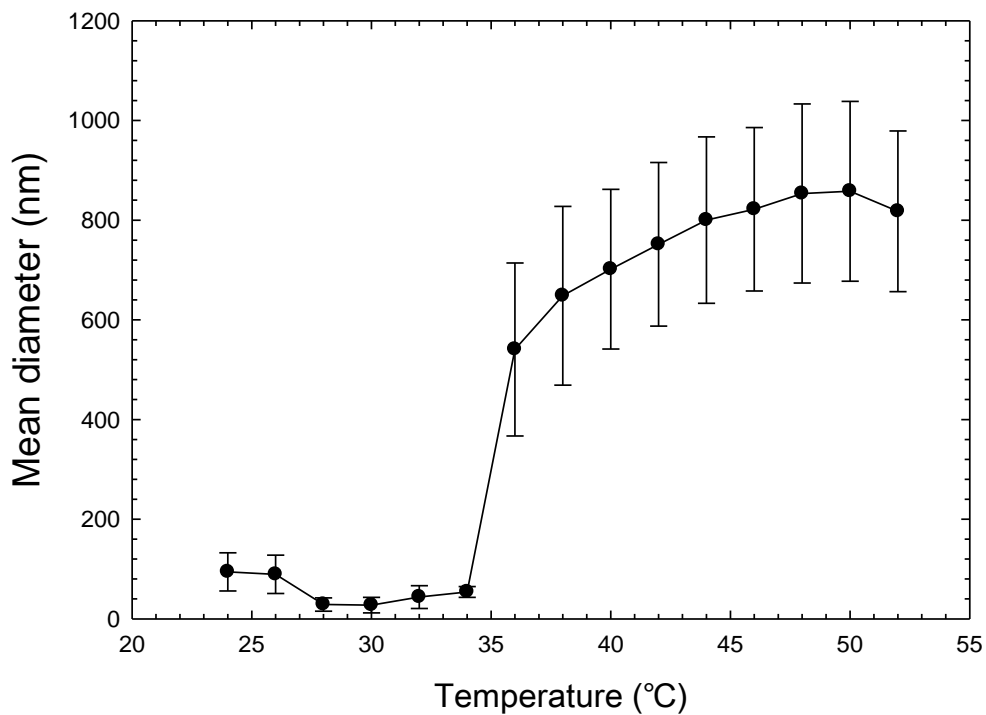


Figure 4-9 Variation of mean diameter of PPG-bis-adenine nanoparticles with temperature under 4 mg/mL

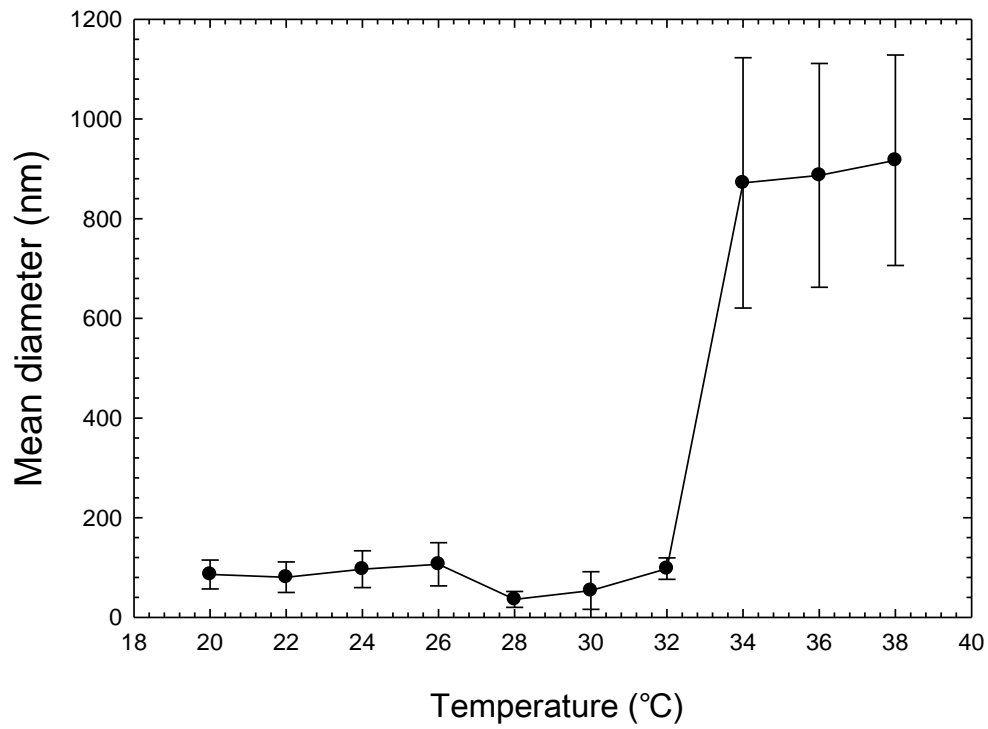


Figure 4-10 Variation of mean diameter of PPG-bis-adenine nanoparticles with temperature under 5 mg/mL

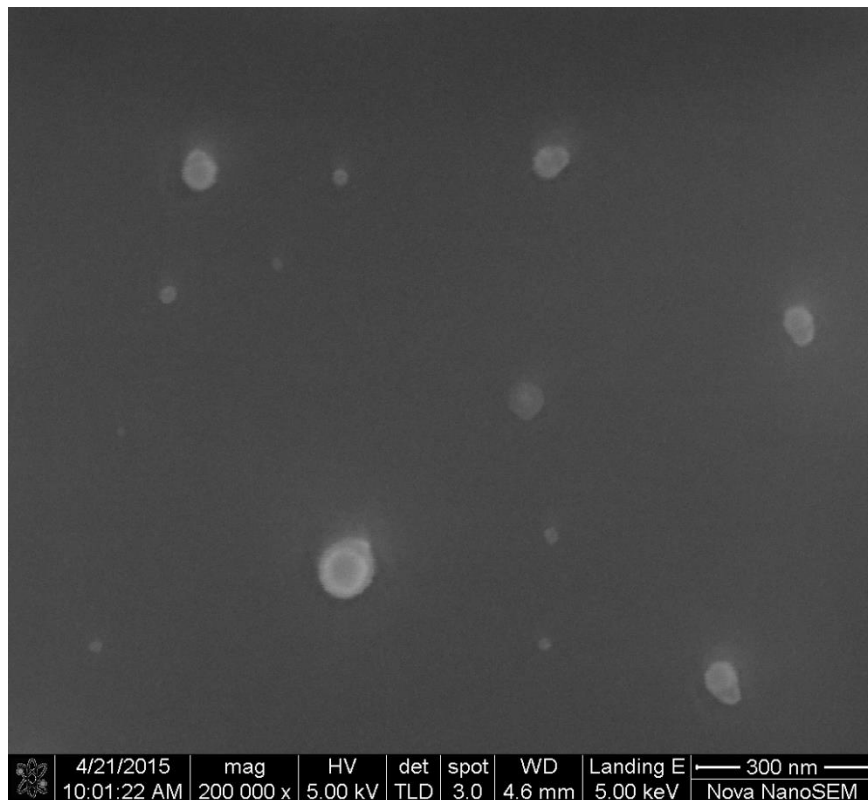


Figure 4-11 SEM image of nanoparticles of PPG-bis-adenine under 1 mg/mL



Figure 4-12 SEM image of nanoparticles of PPG-bis-adenine under 0.1 mg/mL

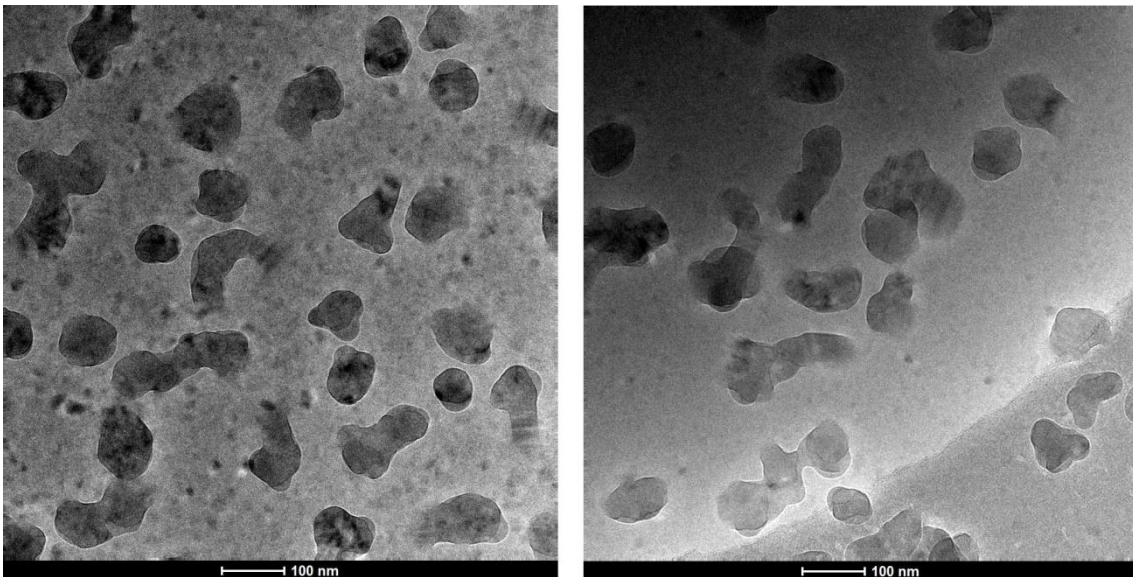


Figure 4-13 Cryo-TEM image of PPG-bis-adenine nanoparticles under 1 mg/mL

4.2.3 Cryo-TEM

Figure 4-13 shows the cryo-TEM image of PPG-bis-adenine nanoparticles under 1 mg/mL. The white lines are artifacts produced by focusing. The black lines should be boundaries of nanoparticles. As observed in SEM images, the nanoparticles are roughly spherical but irregular. The diameter of these nanoparticles is seen to be around 100 nm, which agrees with the result obtained in DLS. This is reasonable, since cryo-TEM samples retain the state when the nanoparticles were in water.

4.2.4 Zeta potential

Zeta potential of 5 different concentrations of PPG-bis-adenine aqueous solution is shown in Figure 4-14. The zeta potential is around -30 mV, indicating that the nanoparticles would only aggregate slightly.



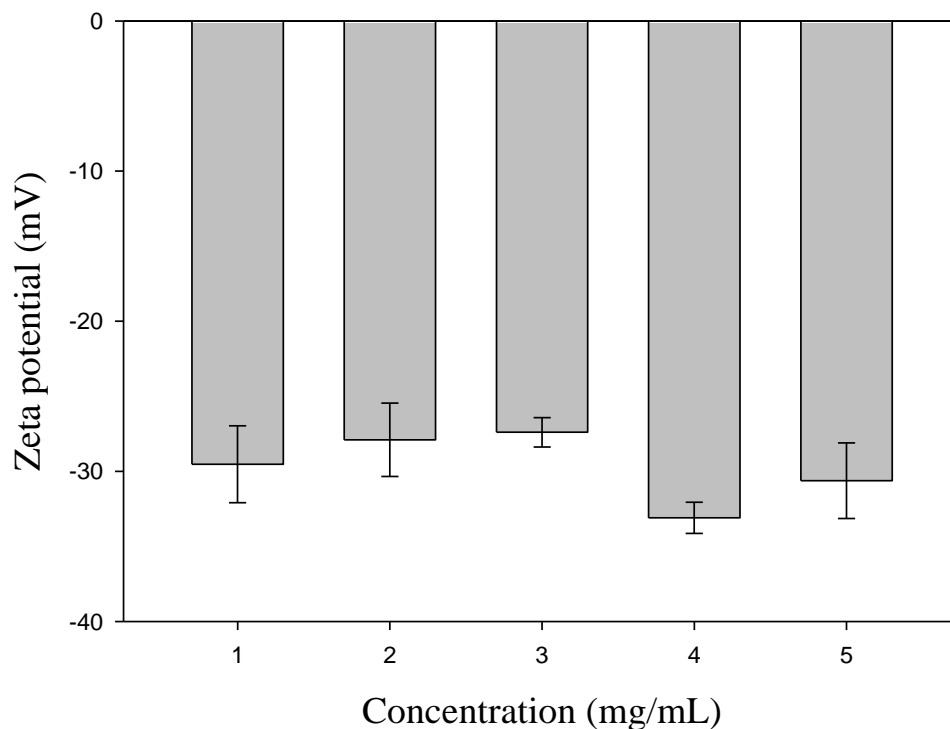


Figure 4-14 Zeta potential of nanoparticles of various concentrations of PPG-bis-adenine aqueous solution

4.2.5 CMC determination

The fluorescent emission spectra of pyrene in different concentration of PPG-bis-adenine solutions are shown in Figure 4-15. The intensity is normalized to 1 at peak I for all spectra. The blue line represents the spectrum of the lowest concentration, and the red line represents the spectrum of the highest concentration, and the spectra of other concentrations are colored in a gradient manner. At lower concentrations, there is no micelle in the solution, and the pyrene is in aqueous (polar) environment. The spectra in aqueous environment have three peaks between 365 and 385 nm, and the ratio of the



intensity of the third peak to that of the first peak are around 0.56.

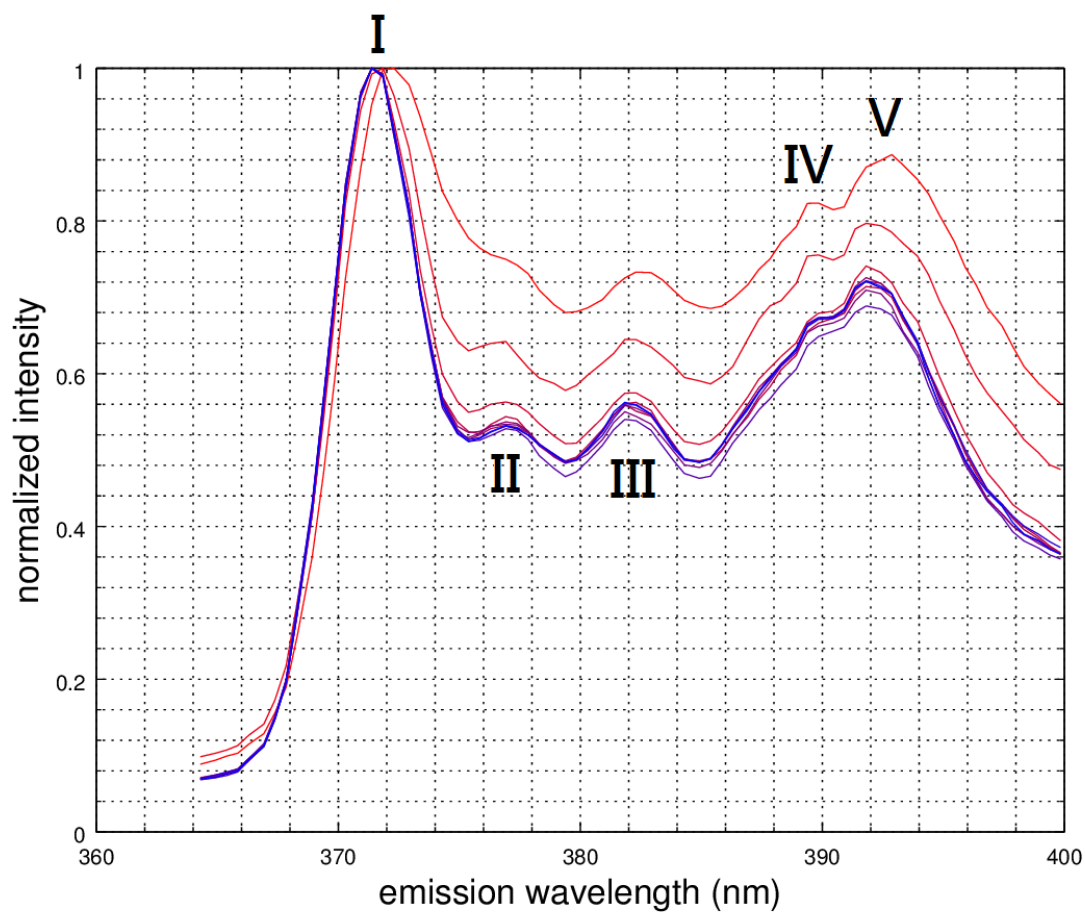


Figure 4-15 Fluorescent emission of pyrene in different concentrations of PPG-bis-adenine solution. The intensity is normalized according to peak I.

At higher concentrations, micelles form in the solution, and pyrene (a non-polar compound) would move into non-polar area of the micelles, experiencing non-polar environment. The three peaks shift to higher wavelength when the concentration increases and the ratio of the intensity of the third peak to that of the first peak also increases from 0.56 to about 0.73.

We can use the “peak III to peak I” ratio to determine the CMC. Figure 4-16 shows the plot of “peak III to peak I ratio” versus the logarithm of concentration. The CMC is estimated to be at the intersection of the two linear regression lines, which is about 8×10^{-2} mg/mL. It should be pointed out that the estimation is somewhat subjective, because the starting point of the increase of slope may be chosen differently. Nevertheless, the CMC determined by this method should be in the range of 0.01 to 0.1 mg/mL, according to the data points of Figure 4-16. There is also a possibility that the actual CMC is lower than estimated here, because there might be too few micelles in the solution for all pyrene molecules to enter when the concentration is just slightly above CMC.

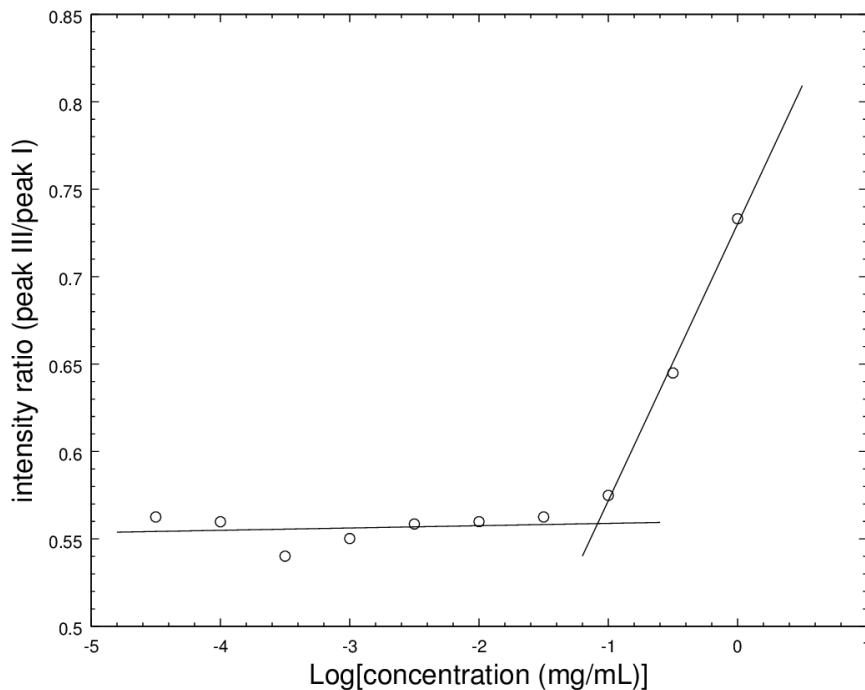


Figure 4-16 CMC determination by the variation of “peak III to peak I” ratio



4.3 The LCST behavior

4.3.1 LCST determination by UV/Vis spectrophotometry

The aqueous solution of PPG-bis-adenine is transparent below LCST. When the temperature is raised above LCST, PPG-bis-adenine becomes insoluble in water, and phase-separates from water to form a cloudy emulsion (Figure 4-20). The change in transmittance is utilized to determine the LCST, and the result is shown in Figure 4-18. The LCST is determined to be the temperature at which the transmittance equals 50%. The LCST of 5, 4, 3, 2, and 1 mg/mL solutions are about 32, 35, 38, 42, and 57°C, respectively (Figure 4-18). The LCST decreases with increasing concentration, and the variation of LCST with temperature becomes smaller when the concentration is higher. Also, the transition of transmittance becomes sharper with increasing concentration. The concentration dependence implies that the LCST of PPG-bis-adenine can be adjusted easily without modification of chain length.

4.3.2 Mean diameter change around LCST

DLS measurement reveals that the mean diameter of nanoparticles of PPG-bis-adenine changes drastically around LCST (Figure 4-19). The mean diameter of the nanoparticles are all around 100 nm below LCST, but are at the order of 1000 nm above LCST.

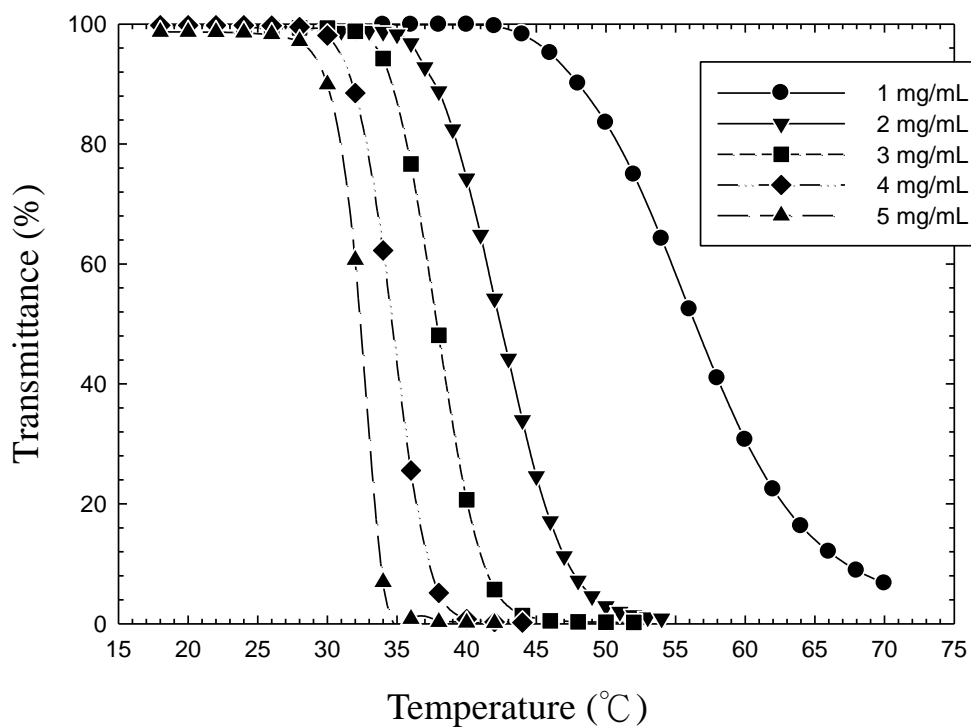


Figure 4-17 LCST determination by transmittance at 800 nm

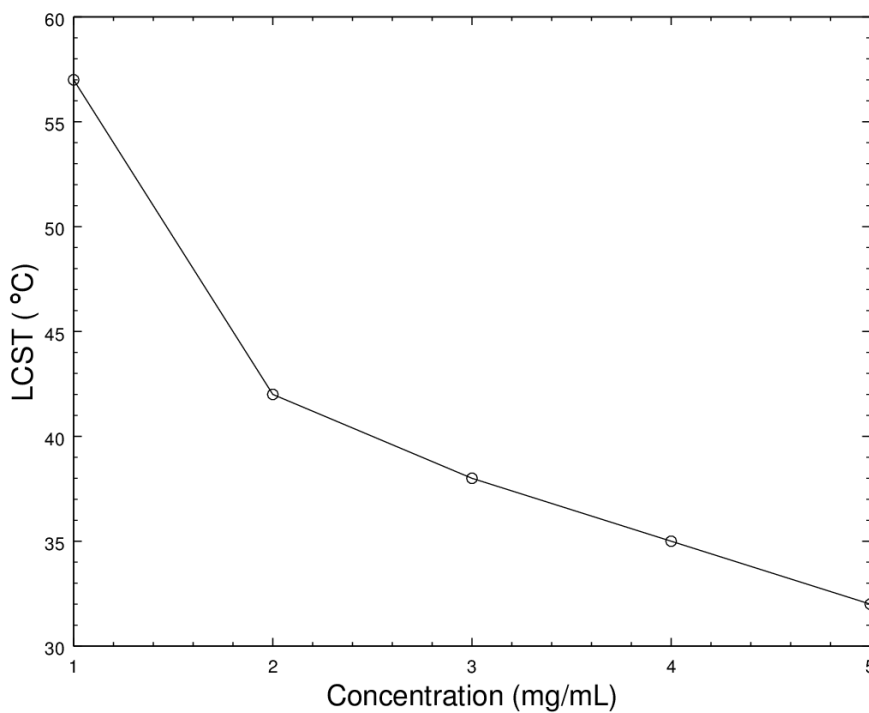


Figure 4-18 Concentration dependence of LCST of PPG-bis-adenine

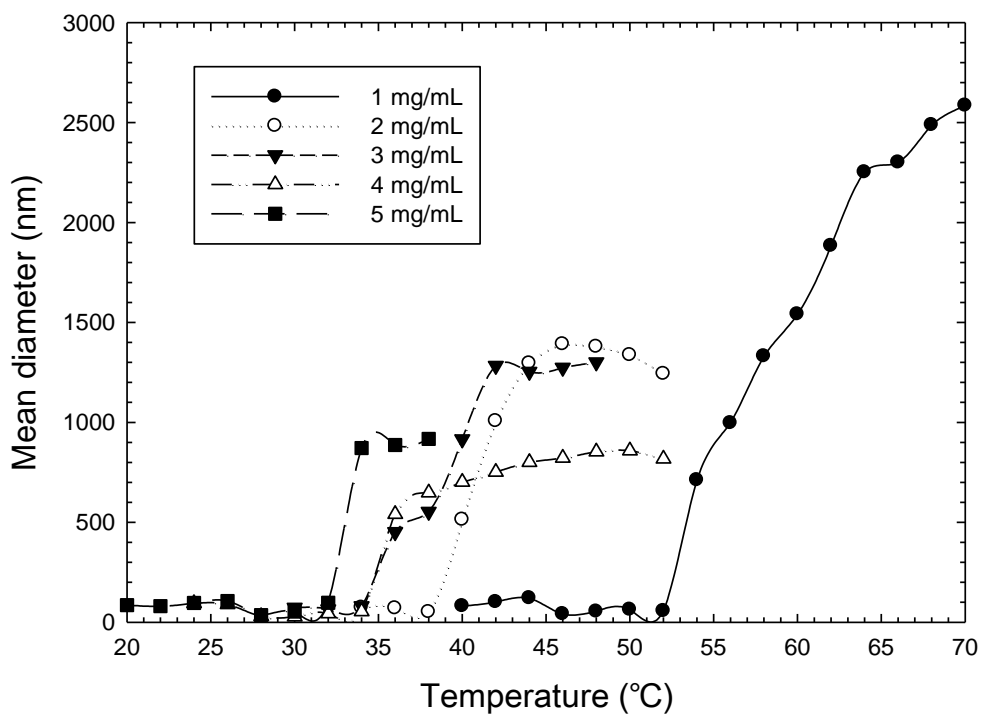


Figure 4-19 Mean diameter variation with temperature across LCST



Figure 4-20 Color change of PPG-bis-adenine solution across LCST



4.4 Drug loading and release

The concentration of pyrene in the ultracentrifugation supernatant of the two drug loading methods was found to be 0.753 and 0.883 times, respectively, of the reference concentration 1.2×10^{-4} mg/mL. The drug entrapment was found to be 87.5% for the first method and 85.3% for the second method, respectively (Figure 4-21). The drug entrapment was almost the same for the two methods, meaning that pyrene could be easily loaded into PPG-bis-adenine nanoparticles simply by mixing them.

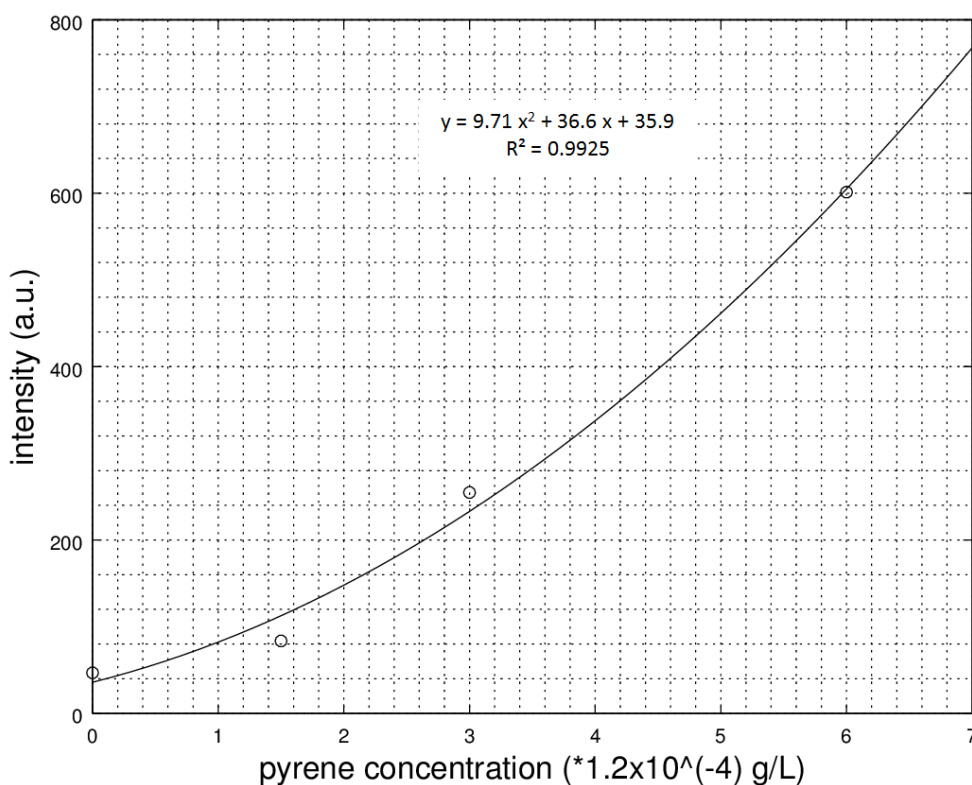
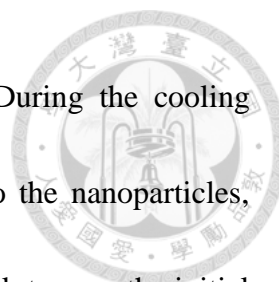


Figure 4-21 Calibration curve for pyrene concentration in drug loading experiment

For the release part, the initial pyrene fluorescent emission intensity was 772 (Figure 4-22, the bold horizontal line). After heating to 50°C, the intensity dropped



down to 521 immediately, signifying instant release of pyrene. During the cooling process, nanoparticles formed again, and pyrene was reloaded into the nanoparticles, which is evident in Figure 4-22, in which the intensity increases back to near the initial intensity.

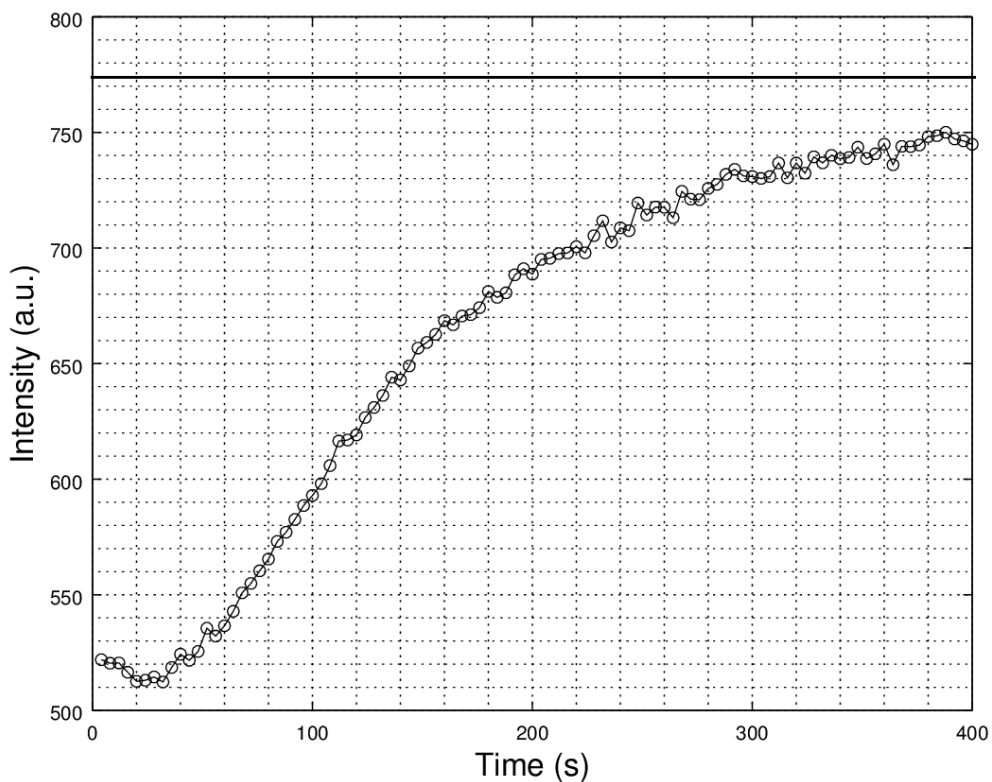


Figure 4-22 Pyrene fluorescent emission intensity change during the release-reload process

Chapter 5. Conclusions and Future work

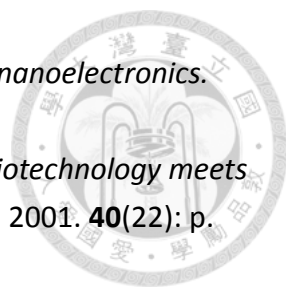


In this study, we have synthesized and characterized the temperature-sensitive material PPG-bis-adenine. Dynamic light scattering, CMC determination, and microscopic images provided the evidence of the existence of nanoparticles, and the mean diameter of the nanoparticles is about 100 nm in aqueous environment under LCST. It exhibits concentration-dependent LCST, whose range covers the body temperature, meaning that the LCST may be adjusted and has the potential to be applied to targeted delivery of cancer drugs. The preliminary drug loading and release experiment showed good entrapment efficiency and instant release at LCST phase change, revealing potential of PPG-bis-adenine as a targeted drug carrier. However, the inner structure of these nanoparticles is yet unclear. The role of hydrogen bonding among adenine moieties and water molecules may be the key to its LCST and drug loading and release behavior. 2D NMR techniques like COSY and NOSEY are needed to explore the effect of hydrogen bonding, and small angle x-ray scattering and atomic force microscopy could be employed to further clarify the mechanism of nanoparticle formation and drug entrapment.




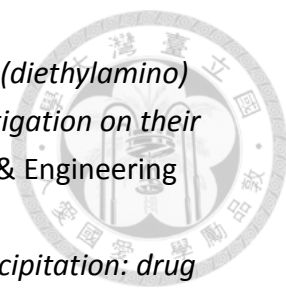
References

- [1] Lehn, J.-M., *Toward complex matter: Supramolecular chemistry and self-organization*. Proceedings of the National Academy of Sciences, 2002. **99**(8): p. 4763-4768.
- [2] Boggs, J.M., *Lipid intermolecular hydrogen bonding: influence on structural organization and membrane function*. Biochimica et Biophysica Acta (BBA)-Reviews on Biomembranes, 1987. **906**(3): p. 353-404.
- [3] Hannon, M.J., *Supramolecular DNA recognition*. Chemical Society Reviews, 2007. **36**(2): p. 280-295.
- [4] Whitesides, G.M., J.P. Mathias, and C.T. Seto, *Molecular self-assembly and nanochemistry: a chemical strategy for the synthesis of nanostructures*. 1991, DTIC Document.
- [5] Whitesides, G.M., et al., *Noncovalent synthesis: using physical-organic chemistry to make aggregates*. Accounts of Chemical Research, 1995. **28**(1): p. 37-44.
- [6] Stang, P.J. and B. Olenyuk, *Self-assembly, symmetry, and molecular architecture: Coordination as the motif in the rational design of supramolecular metallacyclic polygons and polyhedra*. Accounts of chemical research, 1997. **30**(12): p. 502-518.
- [7] Lin, R., et al., *Self-assembly and molecular recognition of a luminescent gold rectangle*. Journal of the American Chemical Society, 2004. **126**(48): p. 15852-15869.
- [8] Ling, X.Y., D.N. Reinhoudt, and J. Huskens, *Reversible attachment of nanostructures at molecular printboards through supramolecular glue*. Chemistry of Materials, 2008. **20**(11): p. 3574-3578.
- [9] Yagai, S., et al., *Unconventional hydrogen-bond-directed hierarchical co-assembly between perylene bisimide and azobenzene-functionalized melamine*. Organic & biomolecular chemistry, 2009. **7**(19): p. 3926-3929.
- [10] Xiao, J., et al., *Self-assembly and optical properties of hydrogen bonded nanostructures containing C 60 and pyrene*. Carbon, 2006. **44**(13): p. 2785-2792.
- [11] Yagai, S., et al., *Structural and Electronic Properties of Extremely Long Perylene Bisimide Nanofibers Formed through a Stoichiometrically Mismatched, Hydrogen-Bonded Complexation*. Small, 2010. **6**(23): p. 2731-2740.

- 
- [12] Gómez-Herrero, J. and F. Zamora, *Coordination polymers for nanoelectronics*. *Advanced Materials*, 2011. **23**(44): p. 5311-5317.
- [13] Niemeyer, C.M., *Nanoparticles, proteins, and nucleic acids: biotechnology meets materials science*. *Angewandte Chemie International Edition*, 2001. **40**(22): p. 4128-4158.
- [14] Janiak, C., *Engineering coordination polymers towards applications*. *Dalton Transactions*, 2003(14): p. 2781-2804.
- [15] Kim, K., et al., *Chiral metal-organic porous materials: synthetic strategies and applications in chiral separation and catalysis*, in *Functional Metal-Organic Frameworks: Gas Storage, Separation and Catalysis*. 2010, Springer. p. 115-153.
- [16] Gokel, G.W., W.M. Leevy, and M.E. Weber, *Crown ethers: sensors for ions and molecular scaffolds for materials and biological models*. *Chemical reviews*, 2004. **104**(5): p. 2723-2750.
- [17] Ludwig, R. and N.T.K. Dzung, *Calixarene-based molecules for cation recognition*. *Sensors*, 2002. **2**(10): p. 397-416.
- [18] Späth, A. and B. König, *Molecular recognition of organic ammonium ions in solution using synthetic receptors*. *Beilstein journal of organic chemistry*, 2010. **6**(1): p. 32.
- [19] Bryan, J.C., et al., *Cesium recognition by supramolecular assemblies of 2-benzylphenol and 2-benzylphenolate*. *Structural Chemistry*, 1999. **10**(3): p. 187-203.
- [20] Ai, K., Y. Liu, and L. Lu, *Hydrogen-bonding recognition-induced color change of gold nanoparticles for visual detection of melamine in raw milk and infant formula*. *Journal of the American Chemical Society*, 2009. **131**(27): p. 9496-9497.
- [21] Merisko-Liversidge, E., G.G. Liversidge, and E.R. Cooper, *Nanosizing: a formulation approach for poorly-water-soluble compounds*. *European Journal of Pharmaceutical Sciences*, 2003. **18**(2): p. 113-120.
- [22] Pouton, C.W., *Formulation of poorly water-soluble drugs for oral administration: physicochemical and physiological issues and the lipid formulation classification system*. *European Journal of Pharmaceutical Sciences*, 2006. **29**(3): p. 278-287.
- [23] Hauss, D.J., *Oral lipid-based formulations*. *Advanced Drug Delivery Reviews*, 2007. **59**(7): p. 667-676.
- [24] Leuner, C. and J. Dressman, *Improving drug solubility for oral delivery using solid dispersions*. *European journal of Pharmaceutics and Biopharmaceutics*, 2000. **50**(1): p. 47-60.
- [25] Merisko-Liversidge, E.M. and G.G. Liversidge, *Drug nanoparticles: formulating*

- poorly water-soluble compounds*. Toxicologic pathology, 2008. **36**(1): p. 43-48.
- [26] Rosenholm, J.M., et al., *Targeted intracellular delivery of hydrophobic agents using mesoporous hybrid silica nanoparticles as carrier systems*. Nano letters, 2009. **9**(9): p. 3308-3311.
- [27] Yi, Q. and G.B. Sukhorukov, *UV light stimulated encapsulation and release by polyelectrolyte microcapsules*. Advances in colloid and interface science, 2014. **207**: p. 280-289.
- [28] Sato, K., et al., *pH-and sugar-sensitive layer-by-layer films and microcapsules for drug delivery*. Advanced drug delivery reviews, 2011. **63**(9): p. 809-821.
- [29] Song, J., et al., *Electrochemically controlled release of molecular guests from redox responsive polymeric multilayers and devices*. European polymer journal, 2013. **49**(9): p. 2477-2484.
- [30] Zhu, S., Z. Zhou, and D. Zhang, *Control of Drug Release through the In Situ Assembly of Stimuli-Responsive Ordered Mesoporous Silica with Magnetic Particles*. ChemPhysChem, 2007. **8**(17): p. 2478-2483.
- [31] He, Q., et al., *An anticancer drug delivery system based on surfactant-templated mesoporous silica nanoparticles*. Biomaterials, 2010. **31**(12): p. 3335-3346.
- [32] Popova, M.D., et al., *Carboxylic modified spherical mesoporous silicas as drug delivery carriers*. International journal of pharmaceutics, 2012. **436**(1): p. 778-785.
- [33] Du, J. and S.P. Armes, *pH-responsive vesicles based on a hydrolytically self-cross-linkable copolymer*. Journal of the American Chemical Society, 2005. **127**(37): p. 12800-12801.
- [34] Banerjee, R. and D. Dhara, *Functional group-dependent self-assembled nanostructures from thermo-responsive triblock copolymers*. Langmuir, 2014. **30**(14): p. 4137-4146.
- [35] Achilleos, D.S., T.A. Hatton, and M. Vamvakaki, *Light-regulated supramolecular engineering of polymeric nanocapsules*. Journal of the American Chemical Society, 2012. **134**(13): p. 5726-5729.
- [36] Danhier, F., O. Feron, and V. Préat, *To exploit the tumor microenvironment: passive and active tumor targeting of nanocarriers for anti-cancer drug delivery*. Journal of Controlled Release, 2010. **148**(2): p. 135-146.
- [37] Cho, K., et al., *Therapeutic nanoparticles for drug delivery in cancer*. Clinical cancer research, 2008. **14**(5): p. 1310-1316.
- [38] Southall, N.T., K.A. Dill, and A. Haymet, *A view of the hydrophobic effect*. The Journal of Physical Chemistry B, 2002. **106**(3): p. 521-533.
- [39] Chandler, D., *Interfaces and the driving force of hydrophobic assembly*. Nature,

- 
2005. **437**(7059): p. 640-647.
- [40] Israelachvili, J.N., *Intermolecular and Surface Forces: With Applications to Colloidal and Biological Systems (Colloid Science)*. 1985, Academic press London.
- [41] Israelachvili, J.N., D.J. Mitchell, and B.W. Ninham, *Theory of self-assembly of hydrocarbon amphiphiles into micelles and bilayers*. Journal of the Chemical Society, Faraday Transactions 2: Molecular and Chemical Physics, 1976. **72**: p. 1525-1568.
- [42] Salim, M., et al., *Amphiphilic designer nano-carriers for controlled release: from drug delivery to diagnostics*. MedChemComm, 2014. **5**(11): p. 1602-1618.
- [43] Smart, T., et al., *Block copolymer nanostructures*. Nano Today, 2008. **3**(3): p. 38-46.
- [44] Schild, H., *Poly (N-isopropylacrylamide): experiment, theory and application*. Progress in polymer science, 1992. **17**(2): p. 163-249.
- [45] Ward, M.A. and T.K. Georgiou, *Thermoresponsive polymers for biomedical applications*. Polymers, 2011. **3**(3): p. 1215-1242.
- [46] Topp, M., et al., *Thermosensitive micelle-forming block copolymers of poly (ethylene glycol) and poly (N-isopropylacrylamide)*. Macromolecules, 1997. **30**(26): p. 8518-8520.
- [47] Qin, S., et al., *Temperature-Controlled Assembly and Release from Polymer Vesicles of Poly (ethylene oxide)-block-poly (N-isopropylacrylamide)*. Advanced Materials, 2006. **18**(21): p. 2905-2909.
- [48] Xu, F., T.-T. Yan, and Y.-L. Luo, *Synthesis and micellization of thermosensitive PNIPAAm-b-PLA amphiphilic block copolymers based on a bifunctional initiator*. Macromolecular Research, 2011. **19**(12): p. 1287-1295.
- [49] Qiao, P., et al., *Synthesis of thermosensitive micelles based on poly (N-isopropylacrylamide) and poly (l-alanine) for controlled release of adriamycin*. Chemical Engineering Journal, 2010. **159**(1): p. 257-263.
- [50] Maeda, Y., T. Nakamura, and I. Ikeda, *Hydration and phase behavior of poly (N-vinylcaprolactam) and poly (N-vinylpyrrolidone) in water*. Macromolecules, 2002. **35**(1): p. 217-222.
- [51] Sun, J., et al., *Effect of Molecular Structure on Thermoresponsive Behaviors of Pyrrolidone-Based Water-Soluble Polymers*. Macromolecules, 2010. **43**(9): p. 4041-4049.
- [52] Yu, Y.C., H.U. Kang, and J.H. Youk, *Synthesis and micellar characterization of thermosensitive amphiphilic poly (ϵ -caprolactone)-b-poly (N-vinylcaprolactam) block copolymers*. Colloid and Polymer Science, 2012. **290**(12): p. 1107-1113.

- 
- [53] Çakal, E.i. and S. Cavus, *Novel poly (N-vinylcaprolactam-co-2-(diethylamino) ethyl methacrylate) gels: characterization and detailed Investigation on their stimuli-sensitive behaviors and network structure*. Industrial & Engineering Chemistry Research, 2010. **49**(22): p. 11741-11751.
- [54] Govender, T., et al., *PLGA nanoparticles prepared by nanoprecipitation: drug loading and release studies of a water soluble drug*. Journal of Controlled Release, 1999. **57**(2): p. 171-185.
- [55] Bohr, A., et al., *Release profile and characteristics of electrosprayed particles for oral delivery of a practically insoluble drug*. Journal of The Royal Society Interface, 2012: p. rsif20120166.
- [56] Li, J., et al., *Preparation and characterization of thermosensitive and biodegradable PNDH-g-PLLA nanoparticles for drug delivery*. Reactive and Functional Polymers, 2009. **69**(12): p. 870-876.
- [57] Chen, W. and J. Du, *Ultrasound and pH dually responsive polymer vesicles for anticancer drug delivery*. Scientific reports, 2013. **3**.
- [58] Du, J., L. Fan, and Q. Liu, *pH-sensitive block copolymer vesicles with variable trigger points for drug delivery*. Macromolecules, 2012. **45**(20): p. 8275-8283.
- [59] Higuchi, T., *Mechanism of sustained-action medication. Theoretical analysis of rate of release of solid drugs dispersed in solid matrices*. Journal of pharmaceutical sciences, 1963. **52**(12): p. 1145-1149.
- [60] Ramyadevi, D. and K.S. Rajan, *Synthesis of hybrid polymer blend nanoparticles and incorporation into in situ gel foam spray for controlled release therapy using a versatile synthetic purine nucleoside analogue antiviral drug*. RSC Advances, 2015. **5**(17): p. 12956-12973.
- [61] Mortensen, K. and J.S. Pedersen, *Structural study on the micelle formation of poly (ethylene oxide)-poly (propylene oxide)-poly (ethylene oxide) triblock copolymer in aqueous solution*. Macromolecules, 1993. **26**(4): p. 805-812.
- [62] Kresheck, G. and F. Franks, *Water, A Comprehensive Treatise, in Aqueous solutions of Amphiphiles and Macromolecules*. 1975, Plenum Press NY. p. 618.
- [63] Kalyanasundaram, K. and J. Thomas, *Environmental effects on vibronic band intensities in pyrene monomer fluorescence and their application in studies of micellar systems*. Journal of the American Chemical Society, 1977. **99**(7): p. 2039-2044.
- [64] Aguiar, J., et al., *On the determination of the critical micelle concentration by the pyrene 1: 3 ratio method*. Journal of Colloid and Interface Science, 2003. **258**(1): p. 116-122.
- [65] Dong, D.C. and M.A. Winnik, *The Py scale of solvent polarities*. Canadian journal

- of chemistry, 1984. **62**(11): p. 2560-2565.
- [66] Zhao, C.L., et al., *Fluorescence probe techniques used to study micelle formation in water-soluble block copolymers*. Langmuir, 1990. **6**(2): p. 514-516.
- [67] Piñeiro, L., M. Novo, and W. Al-Soufi, *Fluorescence emission of pyrene in surfactant solutions*. Advances in colloid and interface science, 2015. **215**: p. 1-12.

